iScience

CellPress
OPEN ACCESS

Article

Exposure to Air Pollution Disrupts Circadian Rhythm through Alterations in Chromatin Dynamics

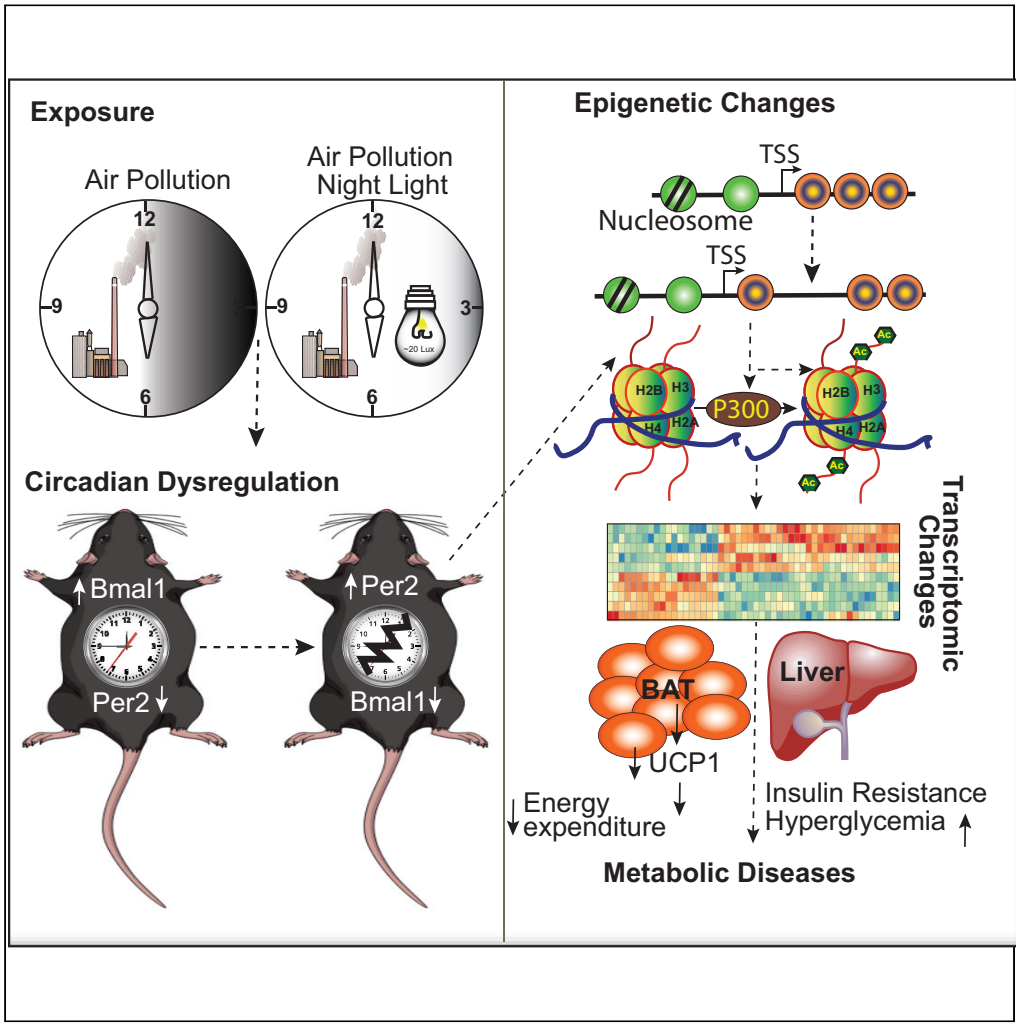

Rengasamy Palanivel, Vinesh Vinayachandran, Shyam Biswal, ..., Mukesh K. Jain, Sujata Rao, Sanjay Rajagopalan

sxr647@case.edu

HIGHLIGHTS

Air pollution disrupts the circadian rhythm (CR) similar to light at night

Dysregulated circadian genes result in insulin resistance and metabolic diseases

$PM_{2.5}$ alters chromatin structure of circadian genes at regulatory regions

$PM_{2.5}$ alters chromatin structure by recruiting histone acetyl transferase (HAT), p300

Palanivel et al., iScience 23, 101728
November 20, 2020 © 2020
https://doi.org/10.1016/j.isci.2020.101728

iScience

CellPress
OPEN ACCESS

Article

Exposure to Air Pollution Disrupts Circadian Rhythm through Alterations in Chromatin Dynamics

Rengasamy Palanivel,[1,9] Vinesh Vinayachandran,[1,9] Shyam Biswal,[2] Jeffrey A. Deiuliis,[1] Roshan Padmanabhan,[6] Bongsoo Park,[2] Roopesh Singh Gangwar,[1] Jared C. Durieux,[3] Elaine Ann Ebreo Cara,[1] Lopa Das,[1] Graham Bevan,[1] Zahi A. Fayad,[7] Ahmed Tawakol,[8] Mukesh K. Jain,[1,3] Sujata Rao,[4,5] and Sanjay Rajagopalan[1,3,10,*]

SUMMARY

Particulate matter $\leq$2.5μm ($PM_{2.5}$) air pollution is a leading environmental risk factor contributing disproportionately to the global burden of non-communicable disease. We compared impact of chronic exposure to $PM_{2.5}$ alone, or with light at night exposure (LL) on metabolism. $PM_{2.5}$ induced peripheral insulin resistance, circadian rhythm (CR) dysfunction, and metabolic and brown adipose tissue (BAT) dysfunction, akin to LL (with no additive interaction between $PM_{2.5}$ and LL). Transcriptomic analysis of liver and BAT revealed widespread but unique alterations in CR genes, with evidence for differentially accessible promoters and enhancers of CR genes in response to $PM_{2.5}$ by ATAC-seq. The histone deacetylases 2, 3, and 4 were downregulated with $PM_{2.5}$ exposure, with increased promoter occupancy by the histone acetyltransferase p300 as evidenced by ChIP-seq. These findings suggest a previously unrecognized role of $PM_{2.5}$ in promoting CR disruption and metabolic dysfunction through epigenetic regulation of circadian targets.

INTRODUCTION

Air pollution is a leading environmental risk factor contributing disproportionately to the global burden of non-communicable diseases (NCDs) (Landrigan et al., 2018). The particulate matter $\leq$2.5 μm in diameter ($PM_{2.5}$) component is the most extensively studied component, with evidence from epidemiological and empirical studies implicating it in the development of insulin resistance (IR) and type II diabetes (T2D) (Munzel et al., 2017b; Rajagopalan et al., 2018). Studies to date have implicated inflammation, oxidative stress, and metabolic dysfunction in response to inhaled $PM_{2.5}$ as broad pathways underlying air pollution effects. However, integrated mechanistic insights are currently lacking (Munzel et al., 2017a).

The circadian system is an evolutionarily conserved system that allows organisms to anticipate predictable environmental changes through coordinated and synchronized changes in behavior and physiology (Bass and Lazar, 2016). The system typically entails entrainment of the internal clock to external environmental cues, so that the rhythmicity of physiological and behavioral processes align with the periodicity of the external environment (Partch et al., 2014). At a molecular level, a central feature of the circadian system is the transcriptional translational feedback loop, involving the core clock genes (Clock, Bmal1, Period 1–3 [*Per1, Per2,* and *Per3*] and Cryptochrome 1–2 [*Cry1* and *Cry2*]) that are transcribed rhythmically and are part of this feedback loop (Bass and Lazar, 2016; Koike et al., 2012; Partch et al., 2014). Given the importance of continuous light as a classic circadian disruptor, we were interested in comparing the effect of $PM_{2.5}$ on continuous light (regular day light at day time and dim light at night time; LL) versus control ambient light conditions (regular day light at day time and dark at night time; LD).

Given that many clock genes are epigenetic regulators, we were particularly interested in comparing the effects of $PM_{2.5}$ and light exposure on chromatin dynamics as a potential mechanism by which environmental triggers may exert broad influence on a range of transcriptional targets (Aubrecht et al., 2015; Bedrosian et al., 2016; Hayashi et al., 2007; Nelson and Chbeir, 2018; Russart and Nelson, 2018). In this study, we exposed mice to chronic inhalation of $PM_{2.5}$, concentrated from ambient air pollution in Cleveland, Ohio.

[1]Cardiovascular Research Institute, Department of Medicine, University Hospitals/Case Western Reserve University, Cleveland, OH, USA

[2]Department of Environmental Health and Engineering, Johns Hopkins University, Baltimore, MD, USA

[3]Harrington Heart and Vascular Institute, University Hospital Cleveland Medical Center, Cleveland, OH, USA

[4]Department of Ophthalmic Research, Cole Eye Institute, Cleveland Clinic, Cleveland, OH 44195, USA

[5]Department of Ophthalmology, Cleveland Clinic Lerner College of Medicine of Case Western Reserve University, Cleveland, OH 44195, USA

[6]Genomic Medicine Institute, Lerner Research Institute, Cleveland Clinic, Cleveland, OH, USA

[7]BioMedical Engineering and Imaging Institute, Icahn School of Medicine at Mount Sinai, New York, NY, USA

[8]Cardiology Division and Cardiovascular Imaging Research Center, Massachusetts General Hospital and Harvard Medical School, Boston, MA, USA

[9]These authors contributed equally

[10]Lead Contact

*Correspondence: sxr647@case.edu

https://doi.org/10.1016/j.isci.2020.101728

The concentration of these ambient particles allowed for exposure levels comparable with air quality in many cities in Asia. Our data provide new evidence on $PM_{2.5}$ exposure-induced metabolic dysfunction through epigenetic regulation of core clock genes.

RESULTS

$PM_{2.5}$ Exposure and Circadian Gene Dysregulation: Discovery Dataset

An initial unbiased RNA sequencing analysis of liver tissue (harvested at ZT02) from male C57BL/6J mice exposed to concentrated $PM_{2.5}$ or filtered air (FA) revealed a significant dysregulation of multiple circadian genes. Exposure to the Versatile Aerosol Concentration Enrichment System (VACES) for 5–6 h a day, 5 days a week for 14 weeks, (n = 12/group) demonstrated downregulation of positive regulators like *Bmal1* and upregulation of negative regulators like *Id1*, *Dbp*, and *Bhlhe4* (Figures S1A and S1B). We conducted a second set of validation experiments to evaluate the comparative and synergistic effects (if any) of $PM_{2.5}$ versus continual light exposure, using a modified VACES system to allow for simultaneous $PM_{2.5}$ exposure and light exposure. C57BL/6J mice at the age of 4 weeks were exposed to FA or concentrated $PM_{2.5}$ for 30 weeks under controlled temperature and humidity as described previously (Figures 1A and S2)Rajagopalan et al., 2020; Sun et al., 2009. The exposure was for 6 h per day with standard light-dark cycle (12 h day light/12 h dark) (LD) or constant light (12 h day light/12 h dim light) (LL), with concomitant *ad libitum* access to standard chow diet. Mean daily $PM_{2.5}$ concentrations inside the chambers were 93.9 ± 25.16 $\mu g/m^3$. Mean daily ambient $PM_{2.5}$ concentrations during the same period in Cleveland were 12.0 ± 3.76 $\mu g/m^3$ (Figure S2A). Mean weekly $PM_{2.5}$ exposure (Figure S2B) and mean elemental concentration (Figure S2D) observed in the VACES system are enumerated. Weekly ambient mean temperature and humidity were also recorded (Figure S2C). Overall, there was approximately an 8-fold enrichment of ambient $PM_{2.5}$.

Chronic Air Pollution ($PM_{2.5}$) Induces Insulin Resistance and Alterations in Energy Homeostasis

We assessed fasting glucose, insulin, and HOMA-IR in the plasma of male mice exposed to either FA or $PM_{2.5}$ under LD or LL conditions for 30 weeks (Figures 1B–1D). $PM_{2.5}$ increased fasting blood glucose levels (Figure 1B) similar to that observed in mice maintained under LL conditions. Importantly LD-$PM_{2.5}$ and LL-FA-exposed mice demonstrated higher plasma insulin and HOMA-IR (Figures 1C and 1D). No changes in body weight and fat mass were noted between the groups (Figures S3A–S3C). Significant differences in glucose tolerance and insulin sensitivity were observed in both LD-FA versus LD-$PM_{2.5}$ (Figures 1E and 1F). As anticipated, LL mice exposed to FA had impaired whole-body glucose tolerance and insulin sensitivity but co-exposure to $PM_{2.5}$ did not result in further exacerbation of phenotype (Figures 1E and 1F). Positron emission tomographic (PET) imaging quantitation of ^{18}F-flurodeoxyglucose (^{18}F-FDG) uptake provides a non-invasive measure of tissue glycolysis. PET imaging revealed ~50% less ^{18}F-FDG uptake within brown adipose tissue (BAT) of LD-$PM_{2.5}$ mice when compared with LD-FA mice (Figures 1G and 1H). ^{18}F-FDG uptake in other tissues such as epididymal white adipose, liver, heart, kidney, and brain were comparable across groups (data not shown). Histological assessment of BAT showed increased "whitening," indicative of lipid and macrophage infiltration, in LD-$PM_{2.5}$ and LL-FA mice, compared with LD-FA mice (Figures 1I and 1J). Expression of the BAT-specific genes *Prdm16* and *Ucp1* (Figures 1K and 1L) was reduced in LD-$PM_{2.5}$ and LL-FA mice. Additionally, Ucp1 protein expression was also reduced (Figure 1M).

$PM_{2.5}$ and LL Alters Stress Hormones, Metabolism, and Circadian Rhythmicity of Core Circadian Genes in Liver and Brown Adipose Tissue

Timed-urinary levels of corticosterone over a 24-h period revealed increased corticosterone at multiple time points with LD-$PM_{2.5}$ versus LD-FA, with a corresponding increase in the aggregate area under curve measurement (Figures S4A and S4B). Periodic corticosterone levels over 24 h in LL-FA exposed mice, although significantly different compared with LD-FA exposed mice (consistent with a circadian disruptor effect of light), was no different from LL-$PM_{2.5}$ exposed mice, suggesting no additional effect of concomitant exposures. Plasma levels of corticosterone and urinary epinephrine, norepinephrine, and dopamine levels were significantly higher in $PM_{2.5}$-exposed mice (Figures S4C–S4F), although these differences were temporally variable, with higher values earlier in the day (zeitgeber time ZT, 02 h) for plasma corticosterone and later in the day for others. Metabolic parameters assessed by indirect calorimetry over 48 h revealed significant reduction in energy expenditure, VO_2 and VCO_2 in LD-$PM_{2.5}$ (Figures 2A, 2C, and 2D). Reduced respiratory exchange ratio (RER) was also noted in LD-$PM_{2.5}$ but only at night (Figure 2B), suggesting that

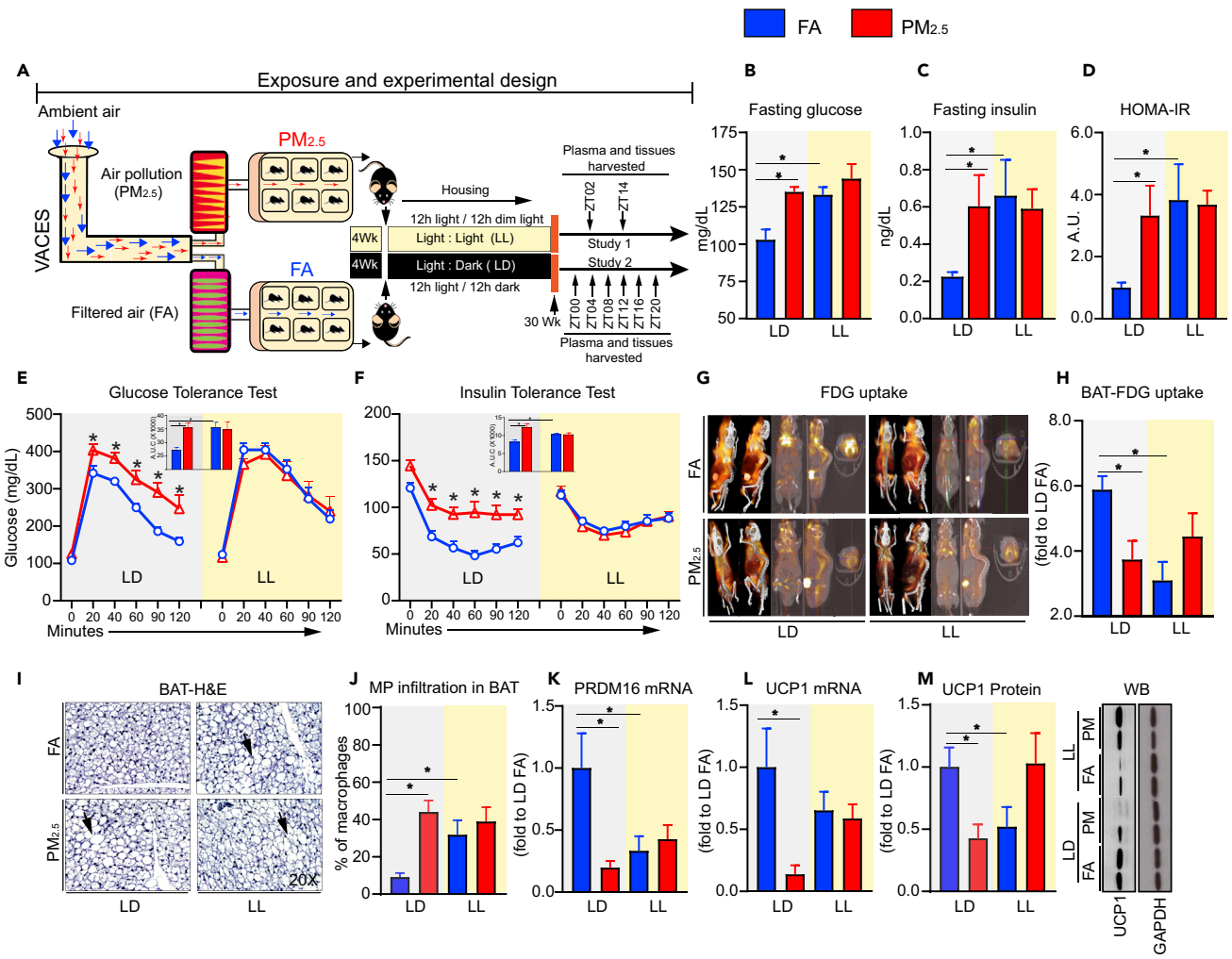

Figure 1. Chronic Air Pollution ($PM_{2.5}$) Induces Insulin Resistance in C57BL/6 Mice

(A–F) (A) Schematic diagram illustrating the exposure and experimental design of the study (wild-type mice were exposed to either filtered air (FA) or $PM_{2.5}$ (6 h/day for 5 days/week) in standard light dark cycle (LD) or constant light (12 h daylight/12 h dim light) (LL) conditions, with concomitant *ad libitum* access to standard chow diet for 30 weeks (Cohort 1: n = 12, Cohort 2: n = 24 per group), (B) fasting blood glucose, (C) fasting insulin, (D) HOMA-IR (overnight fasting before collecting blood) levels as a measure of systemic insulin resistance (n = 12), (E) glucose (2 g/kg) and (F) insulin intolerance test (0.75 U/kg) are summarized by the areas under curve (AUC) following FA, $PM_{2.5}$ exposure (n = 12).

(G–M) (G) representative PET scan images, (H) quantification of standardized FDG uptake in brown fat (SUV), (I) representative image from BAT histology (H&E stain) (n = 5), (J) quantification of percentage of macrophage infiltration in the BAT, (K) mRNA expression of BAT-specific marker *prdm16*, and (L) *UCP1*, (M) quantification of UCP1 protein levels (n = 5) and its representative blot. All data are reported as mean ± SEM. For statistical analysis, p values (*$p < 0.05$) were calculated relative to DAN-FA mice by a two-way analysis of variance (ANOVA) (C and D), one-way ANOVA (E, F, G, J, L, and M) with Tukey's Bonferroni test and by unpaired two-tailed t test (n).

LD-$PM_{2.5}$ mice oxidized fat preferentially at the expense of carbohydrate. Although $PM_{2.5}$ and LL independently altered the above metabolic parameters, in combination they exhibited no additional synergistic effect (data not shown). Significant regulation of genes involved in fatty acid oxidation and gluconeogenesis were noted in both $PM_{2.5}$ and LL exposure, including reduction in PGC1α, PPARα, and CPT1 and upregulation of PEPCK, respectively (Figure S5). LL, but not $PM_{2.5}$, upregulated Acyl-CoA Carboxylase (ACC). However, $PM_{2.5}$ in association with LL increased the ACC expression at ZT14 (Figure S5), associated with CPT1 downregulation, which may then restrict fatty acid entry into the mitochondria for further oxidation. Although no significant changes were observed in pyruvate dehydrogenase kinase isozyme 1 (PDK1) by $PM_{2.5}$, LL, or combination of both (Figure S5) pyruvate dehydrogenase kinase isozyme 4 (PDK4), which also inhibits pyruvate dehydrogenase complex, reducing the conversion of pyruvate from glucose and amino acids to acetyl-CoA, was markedly upregulated by $PM_{2.5}$ but only in conjunction with LL (Figure S5).

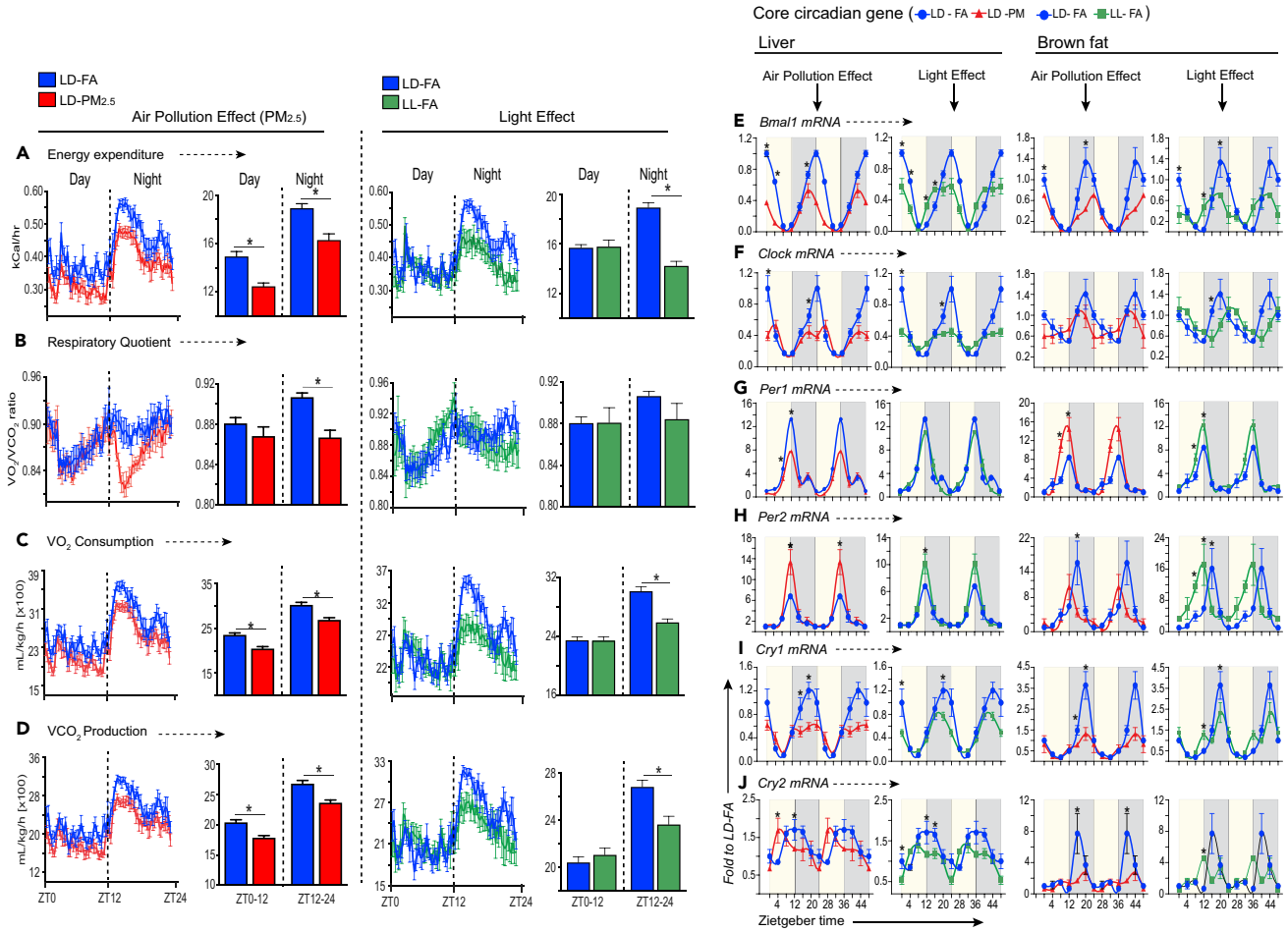

Figure 2. $PM_{2.5}$ Perturbs Resting Energy Expenditure Levels and Peripheral Circadian Rhythm in Wild-Type Mice

Wild-type mice were exposed to FA or $PM_{2.5}$ and light at night (LL) or light at day (LD) as described earlier (n = 6 per group). (A) Hourly energy expenditure during light (6 am–6 pm) and dark (6 pm–6 am) cycle and total light and dark energy expenditure level, (B) hourly day/night respiratory quotient ratio (RQ) and total average day and night RQ value, (C) hourly day/night oxygen consumption rate and total day and night average O_2 consumption rate, (D) hourly day/night CO_2 release rate and total day and night average CO_2 release rate. All line graphs show average of light and dark cycle of mice over a 48-h period. Total average day and night energy expenditure (A), respiratory quotient (B), oxygen consumption (C), and carbon dioxide production (D) are depicted in bar graphs. Values are shown as mean ± SEM. Data are expressed as *$p < 0.05$ relative to LD-FA mice as determined by a two-way analysis of variance (ANOVA) with Tukey's multiple comparison test. mRNA levels of (E) *Bmal1*, (F) *Clock*, (G) Period (*Per*) 1, (H) Period (*Per*) 2, (I) Cryptochrome (*Cry*) 1, and (J) Cryptochrome (*Cry*) 2 in both liver and brown fat (see also Figure S6, Tables S1 and S2), monitored over 24 h (for all panels graphs (E–J) are double plotted). Pale yellow background for (E)–(J) represents tissues harvested during day (light phase), whereas gray background represents tissues harvested at night (dark phase). At each ZT time, tissues from each group of mice (n = 4) were used for analysis. Data are expressed (fold to basal LD-FA ZT00) as mean ± SEM, *$p < 0.05$ relative to LD-FA ZT00 mice is determined by a two-way analysis of variance (ANOVA) with Tukey's multiple comparison test.

To determine if $PM_{2.5}$ affects the peripheral circadian clock, mRNA expression of *Bmal1*, *Clock*, *Per1*, *Per2*, Cry1, and *Cry2* was measured in livers and brown adipose tissues at multiple time points. Expression of *Bmal1*, *Clock*, *Per1*, *Per2*, *Cry1*, and *Cry2* in the liver showed a time-dependent variation in the LD-$PM_{2.5}$ mice that was different from that of LD-FA mice (Figures 2E–2J). Cosinor analysis was applied to investigate the presence of a 24-h rhythm. Cosinor analysis depicted a significant circadian rhythmicity in the expression of *Bmal1*, *Clock*, *Per2*, *Cry1*, *and Cry2* transcripts in the liver of LD-FA mice. A significant effect of both $PM_{2.5}$ and LL on cycling as well as other rhythmic parameters like phase, amplitude, and mesor (rhythm adjusted mean) was observed (Figures 2E–2J, Tables S1 and S2). A significant change in response to an intervention was required to have a reduction in amplitude (1/2 the distance between peak and trough) and a change in either mesor and/or acrophase. Using these criteria, we noted changes in cycling in *Bmal1*, *Clock*, and *Cry1* in liver of LD-$PM_{2.5}$ and LL-FA mice when compared with liver of LD-FA mice (Table S1). A phase advance was noted in *Bmal1* and *Cry2* in LD-$PM_{2.5}$ and LL-FA mice compared with control (LD-

FA). Specifically, liver expression of *Bmal1* and *Cry2* was phase advanced by ~4 h in LD-$PM_{2.5}$ mice (Figures 2E and 2J). In LL-FA, the phase of *Bmal1* and *Cry2* was slightly different than LD-$PM_{2.5}$ compared with LD-FA, the phase was advanced by ~4 h in *Bmal1* and ~2 h in *Cry2* (Figures 2E and 2J, TableS1). Loss of circadian rhythmicity of *Clock, Per2, Cry1*, and *Cry2* expression was observed in animals exposed to LD-$PM_{2.5}$; however, in LL-FA only *Per2* and *Cry2* transcripts lost rhythmicity. A significant decrease in mesor value of several core clock genes (*Bmal1*, *Clock*, *Per1*, *Per2*, and *Cry1*) was noted in LD-$PM_{2.5}$ mice. In response to LL, changes in mesor were limited to only three genes in LL-FA (*Bmal1*, *Clock*, and*Cry1*). Furthermore, the amplitudes of *Bmal1*, *Clock*, and *Cry1* were also significantly reduced in the liver of mice exposed to LD-$PM_{2.5}$ and LL-FA (Table S1). However, the amplitude of *Per2* was significantly increased by $PM_{2.5}$ and LL-FA in contrast to change observed in other clock genes with these exposures (Table S1). These results are consistent with loss of cycling of the core circadian mechanism by $PM_{2.5}$ when compared with FA mice. Unexpectedly, the combination of light and $PM_{2.5}$ (except for the amplitude of *Clock* in liver), did not impact mesor, amplitude, or acrophase of core clock genes when compared with light only condition (Table S1, Figure S6). Individually both $PM_{2.5}$ and LL cause a disruption in rhythmicity; however, the combination of light and $PM_{2.5}$ appears to be a stronger entrainment cue for the expression of *Per1* and *Cry1*(Table S1, Figure S6).

There were notable differences in circadian gene expression comparing BAT with liver. LD-FA mice showed significant circadian rhythm (CR) in expression of most of the genes (*Bmal1, Clock, Per2*, and *cry1*) (Table S2). For instance, only a significant circadian rhythm could be detected for *Bmal1 and Cry1* transcript in mice exposed to LD-$PM_{2.5}$ (Figures 2E and 2I, Table S2). None of the other genes exhibited significant cycling according to the zero amplitude test in Cosinor analysis (Table S2). However, analysis of mRNA expression suggests that expression of *Bmal1, Per1, Cry1*, and *Cry2*, but not *Clock* or *Per2*, is significantly reduced in LD-$PM_{2.5}$ mice (Figures 2E–2J, Table S2). $PM_{2.5}$ and LL had complex effects on *Per1* and *Per2* genes in the BAT, which was diametrically opposite to the pattern observed in the liver, i.e., *Per1* was upregulated by both $PM_{2.5}$ and LL-FA in BAT but downregulated by both in the liver, with mRNA expression highest at ZT12 and lowest at ZT24 (Figures 2G and 2H). Both $PM_{2.5}$ as well as LL-FA significantly decreased peak levels of *Cry*1 transcript at ZT20 and *Cry2* transcript at ZT16 in BAT (Figures 2I and 2J and Table S2). In contrast to the liver, the light plus $PM_{2.5}$ stimuli significantly decreased mesor, amplitude, and phase variation of *Bmal1* in BAT (Table S2 and Figure S6A). Although the amplitudes of *Per1, Per2*, and *Cry1* with light plus $PM_{2.5}$ were unchanged, mesor values were significantly different compared with light only condition (Table S2 and Figures S6C–S6E). Phase delay (~4 h) and phase advance (~4 h) were noticed in expression of *Clock* and *Per2* genes, respectively, in LL-FA condition compared with LD-FA (Figures 2F and 2H, Table S2). Like liver, the combination of light and $PM_{2.5}$ appears to be a stronger entrainment cue as seen for the expression of *Per1* and *Cry1* in BAT (Table S2, Figure S6). Overall, our data suggest that $PM_{2.5}$ is comparable with light exposure in causing widespread circadian disruption in the liver and BAT. Our results on circadian gene variations in liver and BAT are different from those recently published (Li et al., 2020; Wang et al., 2020). This could be due to the duration of $PM_{2.5}$ exposure (10 versus 30 weeks in our study, which truly represents a chronic exposure scenario), inclusion of light at night as a positive control comparator, and the unbiased nature of our analysis.

$PM_{2.5}$ Effects on Circadian Transcriptome

In order to investigate downstream pathways affected by exposure to $PM_{2.5}$ and light, we performed RNA-seq of liver isolated from animals exposed to LD-FA, LD-$PM_{2.5}$, LL-FA, and LL-$PM_{2.5}$. A DESeq analysis was used to compute significant changes in gene expression on exposure to $PM_{2.5}$ and LL (Anders and Huber, 2010). Principal component analysis (PCA) revealed the variability across biological replicates and similarity between treatments (Figure 3A). Figure 3B depicts a heatmap of all differentially expressed genes ($\geq$2-fold change) and the top 50 candidate genes differentially regulated by $PM_{2.5}$ as compared with LL. Genes that were significantly different based on p value in at least one pairwise comparison (n = 459) are depicted in the volcano plot (Figure 3C). In order to further isolate the differential impact of $PM_{2.5}$ versus LL exposure, we plotted DEG's in a four-way plot, comparing two variables (pair) at a time. Pairwise comparisons restrict dimensionality of comparison in gene profiling, allowing one to distinguish unique effects of exposure (light versus $PM_{2.5}$) and to understand combinatorial impact. Figures 3D and S7 demonstrate combinatorial impact of exposures and depict DEGs that are uniquely expressed in response to light and $PM_{2.5}$ versus those DEGs that are uniquely responsive to light or $PM_{2.5}$ individually. Figure 3E depicts a Venn diagram demonstrating unique and overlapping DEGs in response to $PM_{2.5}$ and light as well as the Top 100 DEGs. Overall, only 30% of DEGs overlapped between $PM_{2.5}$ and LL, further corroborating our observation on the uniqueness of the phenotypes caused by $PM_{2.5}$ exposure versus light in the liver of chronic $PM_{2.5}$

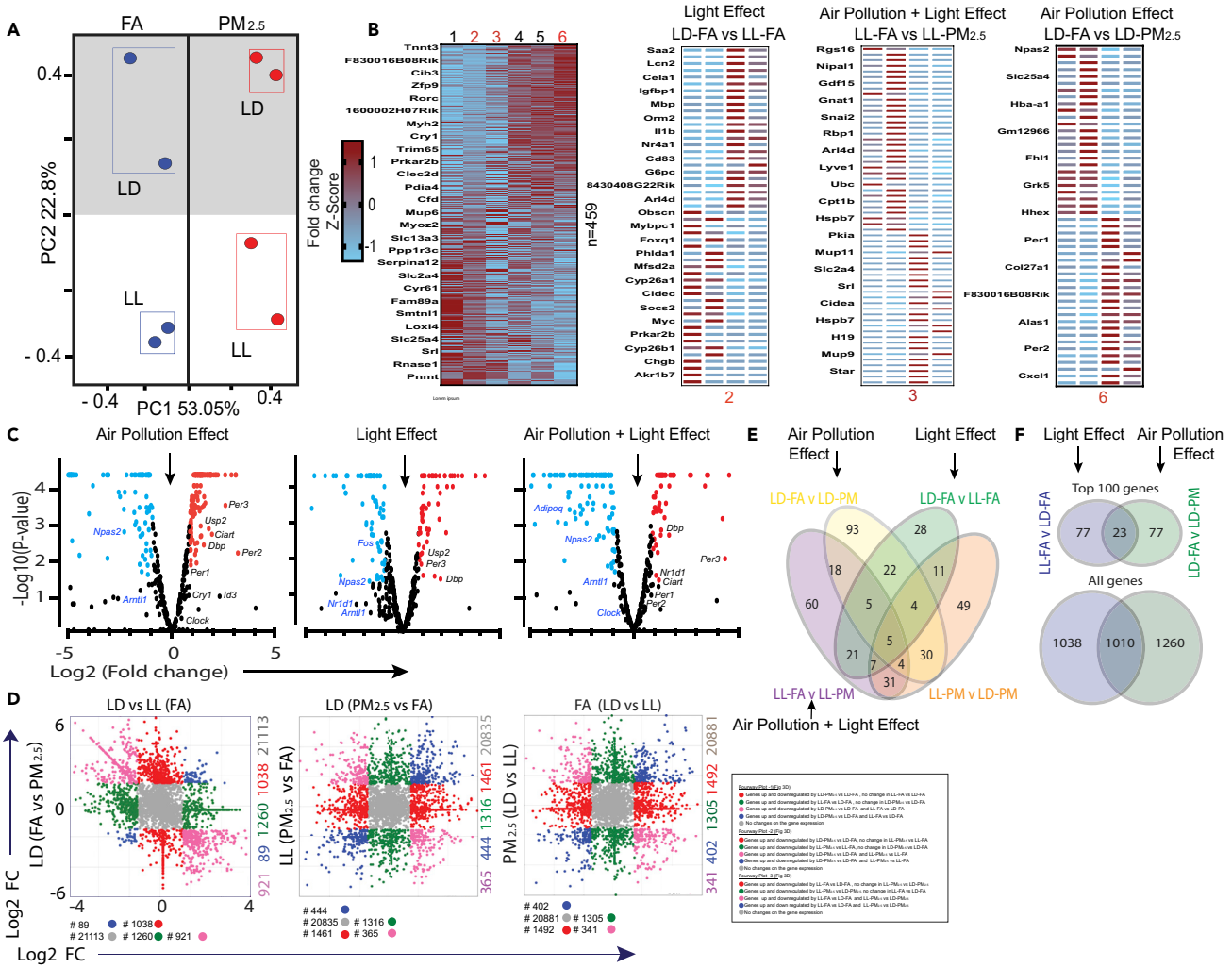

Figure 3. Differential Effect of $PM_{2.5}$ and Light at Night (LL) on Liver Transcriptome

Wild-type mice were exposed to FA or $PM_{2.5}$ (6 h/day for 5 days/week) in standard light dark cycle (LD) or constant light conditions (12 h day light/12 h dim light) (LL) with concomitant *ad libitum* access to standard chow diet for 30 weeks (n = 2 per group).

(A) PCA plot of normalized sequence counts—each circle of same color represents biological replicates of treatments FA/$PM_{2.5}$ and light conditions LL/LD.

(B) Heatmaps of DEGs that are significantly different in at least one pairwise comparison normalized and represented as *Z* scores and each panel represents DEG from one pairwise comparison. Heatmaps of top 50 DEGs based on p values of three different pairwise comparisons in right panel.

(C) Volcano plots showing significantly up- and downregulated differentially expressed circadian/oscillatory genes, labeled in groups that are being compared in the study (see also Figure S7).

(D) Four-way fold change plot shows the DEG in two pairwise comparisons as marked in axes.

(E) Venn diagram indicates the number of overlapping genes between different pairwise comparison.

(F) Venn diagram showing the top 100 DEGs, 30% DEGs overlap between $PM_{2.5}$ and LL.

exposed mice. These results support the idea that the genes affected by two independent environmental circadian disruptors exhibit unique transcriptional signatures.

Expression Profiling of Circadian Genes and Downstream Pathways with $PM_{2.5}$ Exposure

Given the substantial differences in expression profiling in response to two contrasting exposures (light and $PM_{2.5}$), the 459 DEGs that were significant in at least one pairwise comparison from the four different treatment combinations LD (FA versus $PM_{2.5}$), LL (FA versus $PM_{2.5}$) were compared to examine co-regulated genes. In this analysis, the correlation between DEGs reflects the degree of co-regulation, with markedly co-regulated genes depicted in dark blue on heatmaps, with genes with lower co-regulation (correlation)

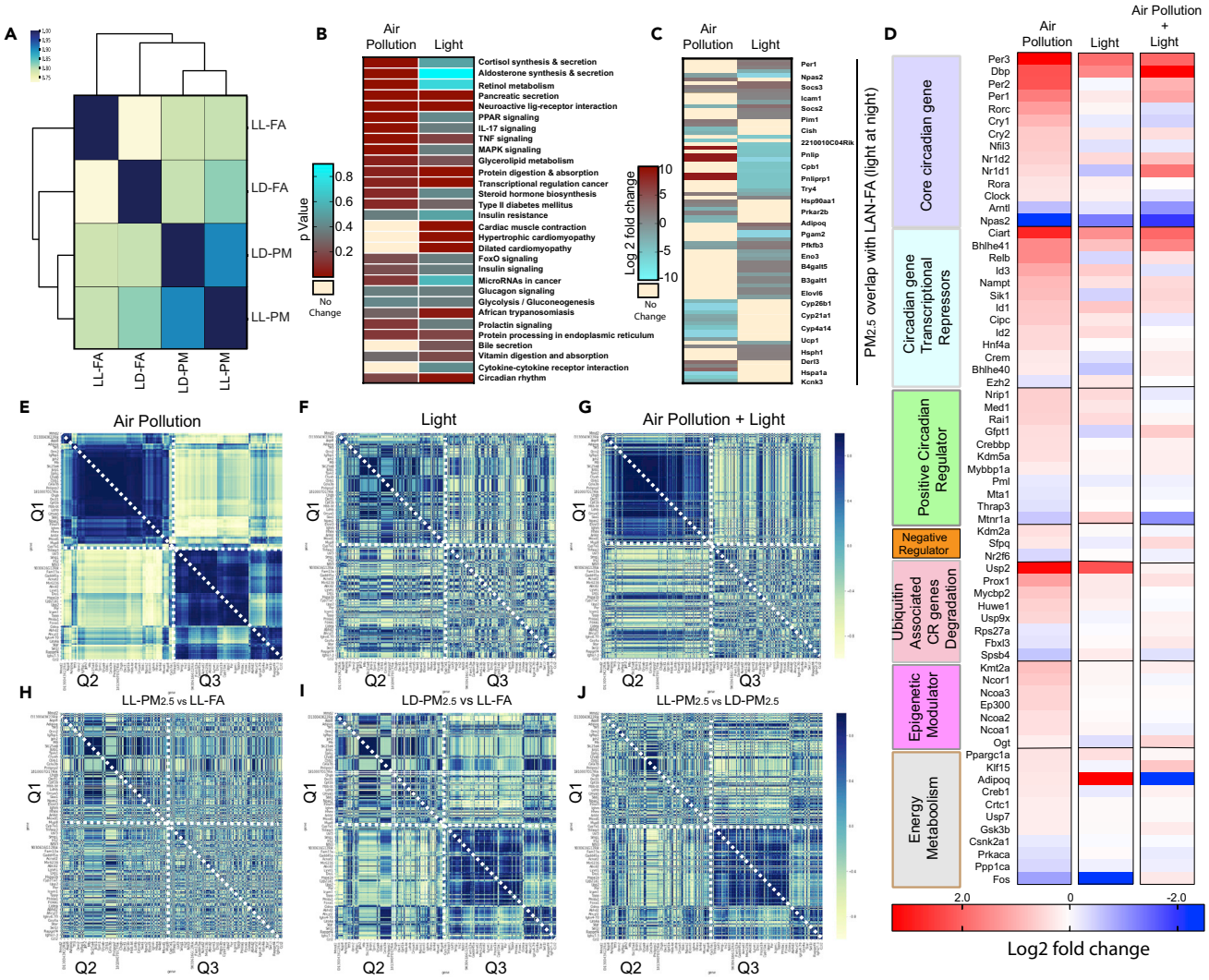

Figure 4. Transcriptomic Signature in the Liver Reveals Positive Correlation between Circadian Disruption, $PM_{2.5}$, and LL

(A) Correlation between pairwise comparisons: dark blue indicates highly correlated, light yellow indicates least correlated.

(B) Heatmap (p value) of circadian pathways disrupted by air pollution and light. Dark red indicates enriched pathways and yellow indicates depleted pathways.

(C) Correlation plots of all DEGs from pairwise comparisons: blue indicates positive correlation and yellow indicates negative correlation.

(D) Heat maps of log2 fold change expression of CR genes divided into seven functional classes under three different conditions—$PM_{2.5}$, LL, and a $PM_{2.5}$ + LL: red indicates high expression (fold change), blue indicates low expression (fold change), whereas cream color indicates no change.

(E–J) Spearman correlation heatmap of DEGs in at least one of the pairwise comparisons: blue indicates high correlation and yellow indicates low correlation to represent the effect of (E) $PM_{2.5}$, (F) light at night, (G) $PM_{2.5}$ and light, (H) $PM_{2.5}$ with light versus FA with light, (I) $PM_{2.5}$ at dark versus FA at light, (J) $PM_{2.5}$ with light versus $PM_{2.5}$ at dark.

shown in cream yellow (Figure 4A). It is apparent that $PM_{2.5}$ exerts a distinctive and greater influence compared with light exposure (LL-FA) based on co-regulated genes. We then turned to other significant pathways regulated in response to $PM_{2.5}$ alone (LD-$PM_{2.5}$) and with light exposure alone (LL-FA, Figure 4B). We selected the top 25 significantly upregulated pathways from I-pathway analysis based on p value cutoff (0.05) and compared these genes within the two groups, with the heatmap representing significantly regulated genes with $PM_{2.5}$ (LD-$PM_{2.5}$ versus LD-FA) and light (LL-$PM_{2.5}$ versus LL-FA, Figure 4C). The top pathways regulated in response to $PM_{2.5}$ included cortisol and aldosterone synthesis, retinol metabolism, and inflammatory signaling (IL-17, TNF, MAPK). These were distinct from pathways regulated in response to LL exposure. However, a number of pathways enriched in response to $PM_{2.5}$ and light also demonstrated concordance and were positively correlated (data not shown). When we analyzed specific genes that

comprised the enriched pathways in Figure 4B, many genes in the enriched pathways in both LD-$PM_{2.5}$ versus FA as well as LL-$PM_{2.5}$ versus LL-FA were not concordant with the pathway (Figure 4C). This implies that genes belonging to the same pathway may exhibit differential regulation depending on the condition and hierarchy in the pathway. Next, we focused specifically on the effect of $PM_{2.5}$, light, and the combination on clusters of core circadian genes and seven classes of oscillatory circadian genes (Figure 4D). The expression of multiple core circadian genes as well as other oscillatory genes were highly regulated in response to both $PM_{2.5}$ and light with no additional impact of the combination. In fact, the combination of LL/PM2.5 exposure seemed to have neutral effects on many core circadian genes and oscillatory circadian gene clusters (Figure 4D). Moreover, an additional correlation analysis (data not shown) revealed a high degree of correlation between $PM_{2.5}$ and light exposure, suggesting possible similarities between the two exposures in causing CR dysfunction.

To examine the co-regulation of DEGs in response to $PM_{2.5}$ and light, we turned to a correlation heatmap that enables pattern recognition in multi-omics assays, by embedding significance of gene expression with gene-gene correlational analysis. In this heatmap, the colors represent the degree of correlation between genes as well as magnitude of expression in response to $PM_{2.5}$ (Figure 4E), light (Figure 4F), and the combination of $PM_{2.5}$ and light (Figure 4G). From this analysis, DEGs in response to $PM_{2.5}$ demonstrated a distinct visual pattern of strongly correlated genes that were confined to three quadrants (Q1, Q2, and Q3). In contrast, light exposure resulted in a pattern that was more diffuse in comparison (Figure 4F). The combination exposure of $PM_{2.5}$ and light (Figure 4G) provided a unique hybrid pattern restricted to Q2, whereas Q1 and Q3 were reminiscent of the predominant pattern of $PM_{2.5}$ (Q1 in Figure 4E) and light (Q3 in Figure 4F). All other combinations of treatments (Figures 4H–4J) were representations that were intermediate between the predominant patterns seen with $PM_{2.5}$ (Figure 4E) and light (Figure 4F), respectively.

$PM_{2.5}$-Mediated Transcriptional Reprograming Involves Alteration of Chromatin Structure

Our transcriptomic analysis suggests that both $PM_{2.5}$ and light mediate broad transcriptional regulation of a multitude of pathways, potentially invoking epigenetic regulation. We performed a genome-wide omni ATAC (ATAC-seq on purified nuclei) on mouse liver exposed to 30 weeks of $PM_{2.5}$ (Corces et al., 2017). PCA analysis confirmed the consistency of biological replicates (Figure 5A). Heatmap sorted based on occupancy of uniquely mapped reads, covering all protein coding genes, is depicted in Figure 5B. We depicted the openness of promoters of top 10% (n = 370) of highly "occupied" core and oscillatory circadian genes as a composite heatmap (Figure 5C) under control conditions (LD-FA, where the intensity of magenta is an indication of active transcription, whereas lighter shades suggest closed chromatin structure indicative of repressive transcription). Our results show that irrespective of light, $PM_{2.5}$ exposure results in an open configuration of the promoter regions of CR genes (Figure 5C). Since differentially accessible open chromatin regions include all classes of *cis*-regulatory elements (promoters, enhancers, and insulators) we sought to determine if $PM_{2.5}$ and light affect all cis-regulatory elements uniformly or if their effects are specific to certain *cis*-regulatory elements (Thurman et al., 2012). Figure 5D depicts the overall distribution of differentially accessible regions (DARs) during $PM_{2.5}$ and light at night exposure seen with $PM_{2.5}$ with enriched and depleted DARs particularly in the intergenic, intronic, 5′ UTR, and 3′ UTR regions. $PM_{2.5}$ had a unique pattern that appeared to be opposite to that observed with LL (Figure 5E). Figure 5F depicts a histogram of all enhancer elements based on exposures. Figure 5G shows that $PM_{2.5}$ exposure induces an open configuration of enhancers (top 10% from http://cirgrdb.biols.ac.cn/), whereas light exposure does not cause any change in configuration.

Chromatin Dynamics in Circadian Genes in Response to $PM_{2.5}$ Is Facilitated by Repressing HDACs

Given that $PM_{2.5}$ effected chromatin dynamics of enhancer elements, we evaluated *Bmal1* binding upon $PM_{2.5}$ and light exposure, given its central role in circadian control and its role as a transcription factor reported to bind to the E-Box elements of multiple genes including other circadian targets (Shostak and Brunner, 2019). Figure 5H depicts that the E-Box spanning motif ($\pm$500 bp) in response to $PM_{2.5}$ exposure is enriched with E-box binding proteins, indicating occupancy of E-box binding proteins, mainly *Bmal1/Clock* (Figure 5H). We investigated the mechanism of altered chromatin dynamics in response to $PM_{2.5}$ exposure and investigated the role of histone acetyl transferases (HATs) and histone deacetylases (HDACs), hypothesizing a reduction in HDACs, or increase in HATs leading to "openness" of chromatin in circadian gene promoters and enhancers. Figure 5I shows a differential regulation of HDACs 2, 3, and 4 transcripts with $PM_{2.5}$ exposures. Combination with light exposure had no additional effect on HDACs. Next, we examined enzymes involved in DNA methylation, such as DNA methyltransferase 1 (DNMT1)

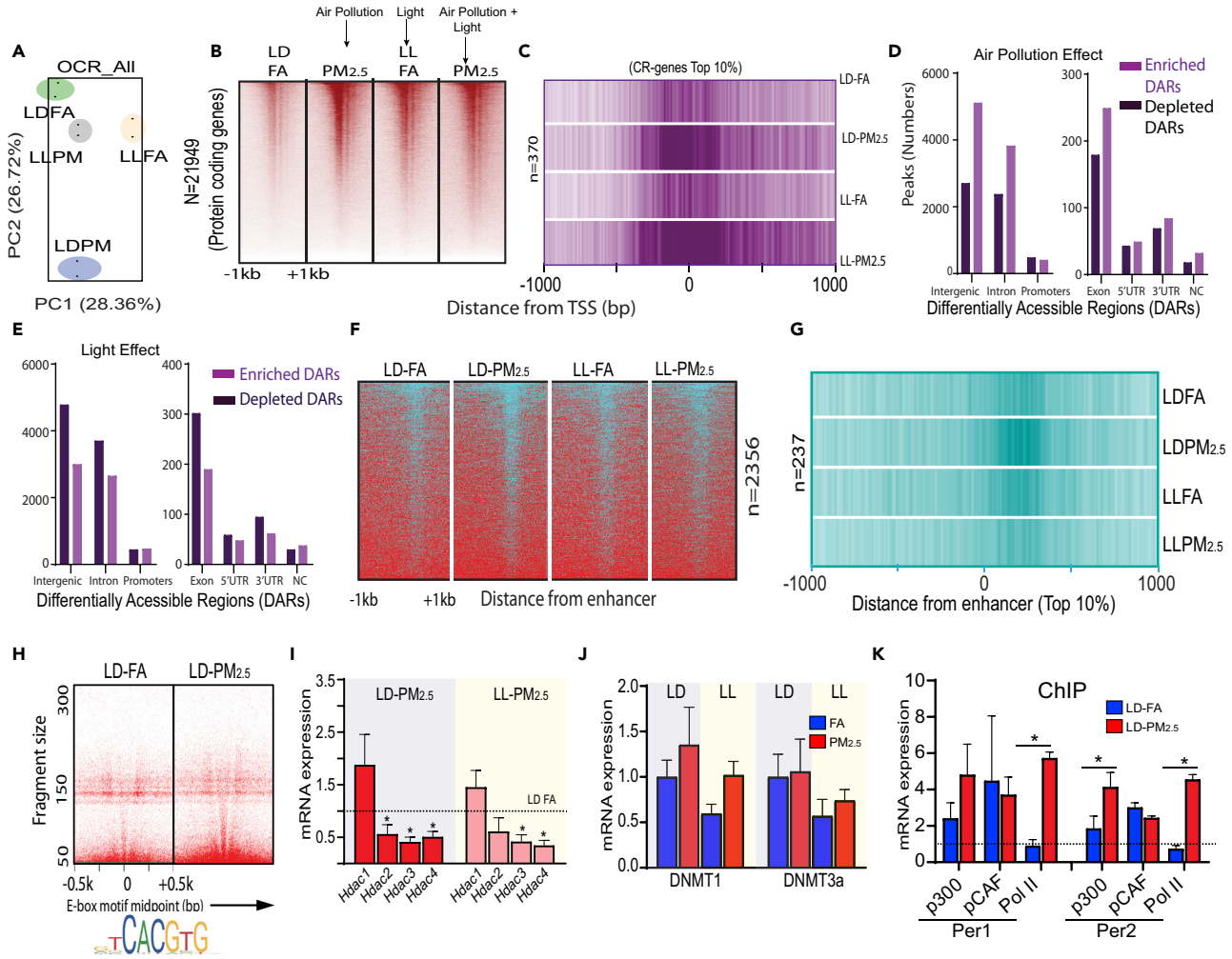

Figure 5. $PM_{2.5}$ Drives Chromatin Structural Changes via Histone Acetylation

(A) PCA plot of normalized sequence counts from ATAC-seq; each colored circle represents biological replicates of treatments labeled as LD FA/LD $PM_{2.5}$ and light conditions as LL FA/LL $PM_{2.5}$; (B) heat maps of normalized sequence tags mapped with respect to transcription start site (TSS) (±1 kb region) of all annotated protein coding gene conditions as mentioned in (A); (C) composite heatmap of top 10% of all oscillatory gene TSS in conditions mentioned in graph with respect to TSS (±1 kb region).

(D–G) (D and E) The distribution of differentially accessible regions (DARs) in different genomic coordinates: dark magenta indicates depleted DARs, whereas light magenta indicates enriched DARs, (F) heatmaps similar to those depicted in (B), but with respect to circadian enhancers, (G) composite map similar to (C), but with respect to top 10% of enhancer midpoints as in the conditions mentioned in axis.

(H–K) (H) V plot mapping the distance from motif mid-point (E-Box) to indicate openness of chromatin structure that is represented by color density of V-line, (I) mRNA expression of HDACs 1–4 in LD and LL groups upon $PM_{2.5}$ exposures, (J) mRNA expression of DNMT1 and DNMT3a in LD and LL upon $PM_{2.5}$ exposures, and (K) Chip-qPCR analysis showing binding of circadian genes *Per1* and *Per2* with p300, PCAF, Pol II.

and 3 alpha (DNMT 3a). Neither $PM_{2.5}$ nor LL made any significant changes on DNMT (1 and 3a) expression (Figure 5J). To identify the HAT responsible for $PM_{2.5}$-specific acetylation of chromatin as a potential mechanism, we performed ChIP-qPCR for p300, pCAF, and polymerase II (Pol II) and probed for their presence in two circadian targets (*Per 1* and *2*), which were upregulated upon $PM_{2.5}$ exposure with resultant increase in openness of *Per1* and *Per2*. We found that the HAT predominantly responsible for acetylating chromatin upon $PM_{2.5}$ exposure is p300 and that these genes were transcriptionally active, indicated by the presence of Pol II.

DISCUSSION

This study provides evidence that chronic ambient air pollution causes disruptions in CR that result in metabolic abnormalities. Specifically, $PM_{2.5}$ exposure induces hyperinsulinemia and BAT dysfunction and results

in altered metabolism (including impaired O_2 consumption and energy expenditure). These phenotypic changes were associated with reprogramming of pathways involved in inflammation, lipid oxidation, and gluconeogenesis, all without changes in body weight. CR disruption was evidenced by marked changes in the rhythmic synthesis of daily corticosteroids, along with changes in amplitude and desynchronization of *Bmal1, Clock, Per1, Per2, Cry1*, and *Cry2* mRNA oscillations in the liver and BAT. Although there were phenotypic similarities between LL and $PM_{2.5}$ exposures, there were also distinct transcriptional and epigenomic differences. Importantly, the effect of light on the transcriptome represented only half of the DEGs when compared with $PM_{2.5}$ or co-exposure to both $PM_{2.5}$ and light at night. Although the magnitude, directionality, and tissue-specific changes were distinct (liver and BAT) for $PM_{2.5}$ and light, a degree of correlation was also noted, suggesting possible similarities between the two exposures in causing CR disruption.

The relationship between CR disruption and metabolic abnormalities (like glucose intolerance, hyperglycemia, and hyperinsulinemia) are well documented (Bedrosian et al., 2016; Gooley, 2016; Krishnaiah et al., 2017; Stenvers et al., 2019). Indeed, CR alterations in metabolism may represent a common denominator for the development of a wide variety of NCDs including cancer and metabolic and cardiovascular disease (Bass and Lazar, 2016; Crnko et al., 2019; Hernandez-Rosas et al., 2020). Recent studies demonstrate that as much as 50% of mouse liver metabolites are under circadian control (Cho et al., 2012; Krishnaiah et al., 2017). Disruption of CR genes has been noted to cause widespread alterations in acetylation and methylation, and conversely, alterations in acetylation and methylation patterns profoundly affect metabolic homeostasis (Kupers et al., 2019; Lombardi et al., 2019; Xia et al., 2015). DNA methylation or phosphorylation of epigenetic modifier proteins has been shown to accompany metabolic stress in mice and humans (Fiedler and Shaw, 2018; Kupers et al., 2019; Liu et al., 2019; Ma et al., 2019). We utilized high-throughput RNA-seq combined with ATAC-seq correlation analysis to interpret aberrantly expressed circadian and metabolic targets in $PM_{2.5}$ exposed mice. $PM_{2.5}$ produced a distinct transcriptional signature compared with LL exposure. There did not appear to be any additive or synergistic effects of LL in addition to $PM_{2.5}$. The expression studies using timed qPCR analysis in liver also demonstrated similarities with the unbiased RNA-seq data in that *Per2* mesor *and* amplitude increased significantly but mesor and amplitudes of all the other core clock genes (*Bmal1*, *Clock*, *Per1*, and *Cry1*) were decreased significantly. Expression of *Bmal1* and *Cry2* was phase advanced in $PM_{2.5}$-exposed mice. A striking feature of RNA-seq expression data in liver in response to $PM_{2.5}$ was the downregulation of core components of the *Bmal1/Npas2* pathways and the upregulation of the negative feedback regulators: *Per1, Per2, Cry1*, and *Cry2*. Despite the observed similarities, the observed differences between differential gene expression profile and cycling analysis of individual core clock genes may be due to the timing differences (multiple time points from ZT0 to ZT24) of tissues harvested for timed PCR analysis, compared with one specific time (ZT02) for harvesting tissues for RNA-seq analysis. In addition, four of the thirteen genes associated with negative regulation of core clock genes, not measured during cycling analysis, were significantly upregulated by $PM_{2.5}$ (*Ciart, Id3, Bhlhe41*, and *Relb*). In particular, Circadian Associated Repressor of Transcription (*Ciart*) or CHRONO (Computationally highlighted repressor of the network oscillator) transcript was highly upregulated in liver by $PM_{2.5}$, with prior studies demonstrating that it represses the transcriptional activity of the *Clock/Bmal1* heterodimer by abrogating the interaction of *Clock/Bmal1* with the transcriptional coactivator *Crebbp* (Anafi et al., 2014; Annayev et al., 2014; Hatanaka and Takumi, 2017).

Circadian oscillations are subject to multiple layers of control. Casein kinase I proteins (CSNK1D and CSNK1E) and F box and leucine-rich repeat proteins like FBXL3 effect the nuclear accumulation and/or stability of clock components, respectively (Busino et al., 2007). Evidence also highlights the importance of epigenetic modification of histone residues (e.g., HDAC3, p300) and DNA methylation histone modifiers in modulating these feedback loops (Asher and Schibler, 2011; Busino et al., 2007). DNA acetylation and methylation are by far the most frequently evaluated epigenetic mechanism (Liu et al., 2015; Rider and Carlsten, 2019). A growing body of evidence implicates that long- and short-term exposures to ambient $PM_{2.5}$ are associated with altered histone acetylation and DNA methylation of genes related to inflammation and cytokines, which results in perturbation of circulating cytokines, and fasting blood glucose (Bind et al., 2014; Chen et al., 2016; Li et al., 2018; Liu et al., 2015). Epigenetic programming in response to environmental exposure may be viewed as a critical and necessary buffer against adverse health response through widespread regulation of gene expression and chromosome integrity (Padmanabhan and Billaud, 2017). Chromatin remodeling may be particularly important with respect to environmental exposures and may help buffer and regulate gene expression (Padmanabhan and Billaud, 2017). Important changes in chromatin dynamics were noted with $PM_{2.5}$, including changes in promoter and enhancer "openness."

E-Box spanning (±500 bp) motifs with $PM_{2.5}$ were enriched in binding proteins, indicating occupancy of E-box binding proteins *Bmal1/Clock*. This was accompanied by differential downregulation of HDACs 2, 3, and 4 transcripts with $PM_{2.5}$ exposure. To identify the HAT responsible for $PM_{2.5}$ specific acetylation of chromatin, ChIP-qPCR for p300, pCAF and polymerase II in two circadian targets (*Per 1* and *2*) were performed. Our data demonstrate that p300 is the candidate HAT and *Per1* and *Per2* were transcriptionally active indicated by the presence of Polymerase II. Thus, increased acetylation could provide an explanation for the metabolic effects of $PM_{2.5}$ exposure. Notably, in a small clinical study (in four individuals, two of whom were exposed to high and two to low $PM_{2.5}$), peripheral blood monocytes among highly exposed individuals showed markedly altered global histone 3 lysine 27 acetylation (H3K27ac, known to be an activation histone modification marker) among highly exposed individuals (Liu et al., 2015). Among differentially modified H3K27ac loci, 1,080 loci were induced in the group with high $PM_{2.5}$, whereas 158 loci were suppressed. The two subjects exposed to high $PM_{2.5}$ tended to have higher number of peaks. H3K27ac peaks overlapped in promoter and enhancer regions, consistent with a role of H3K27ac as a promoter and enhancer marker. Both the TSS and enhancer peaks were higher in the individuals with high $PM_{2.5}$ exposure compared with low-exposed individuals (Liu et al., 2015). CHRONO, which was highly upregulated in liver by $PM_{2.5}$ in our studies, not only represses the transcriptional activity of the *Clock/Bmal1* heterodimer but has also been shown to repress histone acetyltransferase (HAT) activity of the *Clock/Bmal1* heterodimer, reducing histone acetylation of its target genes (Anafi et al., 2014; Annayev et al., 2014; Hatanaka and Takumi, 2017). The mammalian E3 ubiquitin ligase complexes have been shown to specifically regulate the stability of *Per* and *Cry* proteins. FBXL3, a component of the SKP1-CUL1-F-box-protein (SCF) E3 ubiquitin ligase complex, has been reported to target *Cry1* for ubiquitination and an additional molecular component of the negative feedback loop that generates circadian rhythmicity (Busino et al., 2007; Siepka et al., 2007). Loss of FBXL3 activity can thus lead to *Cry* stabilization owing to decreased ubiquitination resulting in downregulation of *Bmal1*. In our study, *Usp2*, another E3 deubiquitinating ligase enzyme, was also highly upregulated in the liver by $PM_{2.5}$. This may represent an additional explanation for the downregulation of the *Bmal1* and *Npas2* that we observed in our study.

Limitations of the Study

We recognize that our data have several important limitations that warrant further investigation including characterization of sexual dimorphism in response to air pollution. In a related study, we showed that females are resistant to $PM_{2.5}$ metabolic effects suggesting that these mechanisms may indeed be relevant (Rajagopalan et al., 2020). Moreover, although food intake is an important synchronizing cue for the clocks of various tissues with essential metabolic roles in peripheral tissues, light is the dominant environmental cue for the suprachiasmatic nucleus master clock that synchronizes the phases of all the other molecular clocks in the body. In the absence of light (the primary zeitgeber), feeding is therefore an ineffective zeitgeber for the SCN. However, feeding has been shown to be a potent zeitgeber for the peripheral circadian rhythm regardless of opposing cues from the light-entrained SCN clock (Pickel and Sung, 2020). The primary goal of our study, therefore, was to explore the interaction between light and air pollution. Even though the mice were not completely restricted for food access during the resting phase (day time), during 6 h of the FA/$PM_{2.5}$ exposure 5 days a week, the mice were unable to access food. However, it will be interesting to determine whether the effects of $PM_{2.5}$ on the liver or BAT circadian rhythms would be abolished with restricted diet in the future. Furthermore, inclusion of methylation analysis of CR genes and their targets and creation of comprehensive epi-genomic maps for air pollution $PM_{2.5}$ exposures are clearly warranted. Additionally, these findings should prompt further investigations into the importance of central versus peripheral CR disruption in mediating the effects of air pollution. In summary, we observed that $PM_{2.5}$ induces hyperinsulinemia and BAT dysfunction and results in altered metabolism and alterations in circadian rhythm genes. These findings suggest a previously unrecognized role of $PM_{2.5}$ in promoting CR disruption and metabolic dysfunction through epigenetic regulation of circadian targets. Well-designed human studies are needed to evaluate the clinical relevance of these pollution-induced alterations on circadian rhythms and health overall.

Resource Availability

Lead Contact

Further information and requests for resources and reagents should be directed to and will be fulfilled by the Lead Contact, Sanjay Rajagopalan (sxr647@case.edu).

Materials Availability

This study did not generate new unique reagents.

Data and Code Availability

The datasets/code (sequencing) generated during this study are available at NCBI Gene Expression Omnibus GEO; http://www.ncbi.nlm.nih.gov/geo/ under accession number GSE145566

METHODS

All methods can be found in the accompanying Transparent Methods supplemental file.

SUPPLEMENTAL INFORMATION

Supplemental Information can be found online at https://doi.org/10.1016/j.isci.2020.101728.

ACKNOWLEDGMENTS

We are grateful to Dr. Chris A. Flask, Associate Professor, Department of Radiology, School of Medicine for determining body fat/water composition (MRI) and for conducting the FDG uptake (PET/CT) study and analysis. We thank Dr. Colleen Croniger, Associate Professor, Department of Nutrition School of Medicine for mice metabolic cage study and analysis. We thank Dr. Brendan Eck, Department of Biomedical Engineering for making 3D images for FDG uptake. We acknowledge Jenifer Mikulan, Institute Pathology for BAT histopathological study. We thank Dr. E Ricky Chan, Institute of Computational Biology, Case Western Reserve University for transcriptome and ATAC-seq analysis. This work was supported by the National Institute of Environmental Health Sciences (NIEHS) of the National Institutes of Health (NIH) under Award Numbers U01ES026721 (to S.B. and S.R.) and 5R01ES019616 and 1RO1ES015146 (to S.R.)

AUTHOR CONTRIBUTIONS

S.Rajagopalan and S.B. conceptualized and initiated $PM_{2.5}$-based exposure design, edited and approved, wrote, and finalized the final manuscript. J.A.D. designed the light at night exposure experiments, edited the manuscript. R.P. and V.V. performed most experiments. E.A.E.C. conducted the circadian gene expression study. R. Padmanabhan and B.P. conducted bioinformatics analysis. R.P., E.A.E.C., R.S.G., L.D., and G.B. conducted PM exposure and tissue collection. R.P. conducted phenotype assays including BAT histology, microscope imaging, and GTT/ITT. V.V. prepared sequencing libraries and performed OMNI ATAC-seq. J.C.D. performed statistical analysis for all experiments. R.P., V.V., and S.R. wrote a draft manuscript. S. Rajagopalan, S. Rao, M.J.K., Z.F., and A.T. contributed to revising and finalizing the manuscript.

DECLARATION OF INTERESTS

The authors declare no competing financial interests.

Received: April 28, 2020
Revised: August 21, 2020
Accepted: October 21, 2020
Published: November 20, 2020

REFERENCES

Anafi, R.C., Lee, Y., Sato, T.K., Venkataraman, A., Ramanathan, C., Kavakli, I.H., Hughes, M.E., Baggs, J.E., Growe, J., Liu, A.C., et al. (2014). Machine learning helps identify CHRONO as a circadian clock component. PLoS Biol. *12*, e1001840.

Anders, S., and Huber, W. (2010). Differential expression analysis for sequence count data. Genome Biol. *11*, R106.

Annayev, Y., Adar, S., Chiou, Y.Y., Lieb, J.D., Sancar, A., and Ye, R. (2014). Gene model 129 (Gm129) encodes a novel transcriptional repressor that modulates circadian gene expression. J. Biol. Chem. *289*, 5013–5024.

Asher, G., and Schibler, U. (2011). Crosstalk between components of circadian and metabolic cycles in mammals. Cell Metab. *13*, 125–137.

Aubrecht, T.G., Jenkins, R., and Nelson, R.J. (2015). Dim light at night increases body mass of female mice. Chronobiol. Int. *32*, 557–560.

Bass, J., and Lazar, M.A. (2016). Circadian time signatures of fitness and disease. Science *354*, 994–999.

Bedrosian, T.A., Fonken, L.K., and Nelson, R.J. (2016). Endocrine effects of circadian disruption. Annu. Rev. Physiol. *78*, 109–131.

Bind, M.A., Lepeule, J., Zanobetti, A., Gasparrini, A., Baccarelli, A., Coull, B.A., Tarantini, L., Vokonas, P.S., Koutrakis, P., and Schwartz, J. (2014). Air pollution and gene-specific methylation in the Normative Aging Study: association, effect modification, and mediation analysis. Epigenetics *9*, 448–458.

Busino, L., Bassermann, F., Maiolica, A., Lee, C., Nolan, P.M., Godinho, S.I., Draetta, G.F., and Pagano, M. (2007). SCFFbxl3 controls the

oscillation of the circadian clock by directing the degradation of cryptochrome proteins. Science *316*, 900–904.

Chen, R., Meng, X., Zhao, A., Wang, C., Yang, C., Li, H., Cai, J., Zhao, Z., and Kan, H. (2016). DNA hypomethylation and its mediation in the effects of fine particulate air pollution on cardiovascular biomarkers: a randomized crossover trial. Environ. Int. *94*, 614–619.

Cho, H., Zhao, X., Hatori, M., Yu, R.T., Barish, G.D., Lam, M.T., Chong, L.W., DiTacchio, L., Atkins, A.R., Glass, C.K., et al. (2012). Regulation of circadian behaviour and metabolism by REV-ERB-alpha and REV-ERB-beta. Nature *485*, 123–127.

Corces, M.R., Trevino, A.E., Hamilton, E.G., Greenside, P.G., Sinnott-Armstrong, N.A., Vesuna, S., Satpathy, A.T., Rubin, A.J., Montine, K.S., Wu, B., et al. (2017). An improved ATAC-seq protocol reduces background and enables interrogation of frozen tissues. Nat. Methods *14*, 959–962.

Crnko, S., Du Pre, B.C., Sluijter, J.P.G., and Van Laake, L.W. (2019). Circadian rhythms and the molecular clock in cardiovascular biology and disease. Nat. Rev. Cardiol. *16*, 437–447.

Fiedler, E.C., and Shaw, R.J. (2018). AMPK regulates the epigenome through phosphorylation of TET2. Cell Metab. *28*, 534–536.

Gooley, J.J. (2016). Circadian regulation of lipid metabolism. Proc. Nutr. Soc. *75*, 440–450.

Hatanaka, F., and Takumi, T. (2017). CHRONO integrates behavioral stress and epigenetic control of metabolism. Ann. Med. *49*, 352–356.

Hayashi, M., Shimba, S., and Tezuka, M. (2007). Characterization of the molecular clock in mouse peritoneal macrophages. Biol. Pharm. Bull. *30*, 621–626.

Hernandez-Rosas, F., Lopez-Rosas, C.A., and Saavedra-Velez, M.V. (2020). Disruption of the molecular circadian clock and cancer: an epigenetic link. Biochem. Genet. *58*, 189–209.

Koike, N., Yoo, S.H., Huang, H.C., Kumar, V., Lee, C., Kim, T.K., and Takahashi, J.S. (2012). Transcriptional architecture and chromatin landscape of the core circadian clock in mammals. Science *338*, 349–354.

Krishnaiah, S.Y., Wu, G., Altman, B.J., Growe, J., Rhoades, S.D., Coldren, F., Venkataraman, A., Olarerin-George, A.O., Francey, L.J., Mukherjee, S., et al. (2017). Clock regulation of metabolites reveals coupling between transcription and metabolism. Cell Metab. *25*, 961–974 e964.

Kupers, L.K., Monnereau, C., Sharp, G.C., Yousefi, P., Salas, L.A., Ghantous, A., Page, C.M., Reese, S.E., Wilcox, A.J., Czamara, D., et al. (2019). Meta-analysis of epigenome-wide association studies in neonates reveals widespread differential DNA methylation associated with birthweight. Nat. Commun. *10*, 1893.

Landrigan, P.J., Fuller, R., Acosta, N.J.R., Adeyi, O., Arnold, R., Basu, N.N., Balde, A.B., Bertollini, R., Bose-O'Reilly, S., Boufford, J.I., et al. (2018). The Lancet Commission on pollution and health. Lancet *391*, 462–512.

Li, H., Chen, R., Cai, J., Cui, X., Huang, N., and Kan, H. (2018). Short-term exposure to fine particulate air pollution and genome-wide DNA methylation: a randomized, double-blind, crossover trial. Environ. Int. *120*, 130–136.

Li, R., Wang, Y., Chen, R., Gu, W., Zhang, L., Gu, J., Wang, Z., Liu, Y., Sun, Q., Zhang, K., et al. (2020). Ambient fine particulate matter disrupts hepatic circadian oscillation and lipid metabolism in a mouse model. Environ. Pollut. *262*, 114179.

Liu, C., Xu, J., Chen, Y., Guo, X., Zheng, Y., Wang, Q., Chen, Y., Ni, Y., Zhu, Y., Joyce, B.T., et al. (2015). Characterization of genome-wide H3K27ac profiles reveals a distinct PM2.5-associated histone modification signature. Environ. Health *14*, 65.

Liu, J., Carnero-Montoro, E., van Dongen, J., Lent, S., Nedeljkovic, I., Ligthart, S., Tsai, P.C., Martin, T.C., Mandaviya, P.R., Jansen, R., et al. (2019). An integrative cross-omics analysis of DNA methylation sites of glucose and insulin homeostasis. Nat. Commun. *10*, 2581.

Lombardi, A.A., Gibb, A.A., Arif, E., Kolmetzky, D.W., Tomar, D., Luongo, T.S., Jadiya, P., Murray, E.K., Lorkiewicz, P.K., Hajnoczky, G., et al. (2019). Mitochondrial calcium exchange links metabolism with the epigenome to control cellular differentiation. Nat. Commun. *10*, 4509.

Ma, J., Nano, J., Ding, J., Zheng, Y., Hennein, R., Liu, C., Speliotes, E.K., Huan, T., Song, C., Mendelson, M.M., et al. (2019). A peripheral blood DNA methylation signature of hepatic fat reveals a potential causal pathway for Nonalcoholic fatty liver disease. Diabetes *68*, 1073–1083.

Munzel, T., Sorensen, M., Gori, T., Schmidt, F.P., Rao, X., Brook, F.R., Chen, L.C., Brook, R.D., and Rajagopalan, S. (2017a). Environmental stressors and cardio-metabolic disease: part II-mechanistic insights. Eur. Heart J. *38*, 557–564.

Munzel, T., Sorensen, M., Gori, T., Schmidt, F.P., Rao, X., Brook, J., Chen, L.C., Brook, R.D., and Rajagopalan, S. (2017b). Environmental stressors and cardio-metabolic disease: part I-epidemiologic evidence supporting a role for noise and air pollution and effects of mitigation strategies. Eur. Heart J. *38*, 550–556.

Nelson, R.J., and Chbeir, S. (2018). Dark matters: effects of light at night on metabolism. Proc. Nutr. Soc. *77*, 223–229.

Padmanabhan, K., and Billaud, M. (2017). Desynchronization of circadian clocks in cancer: a metabolic and epigenetic connection. Front. Endocrinol. (Lausanne) *8*, 136.

Partch, C.L., Green, C.B., and Takahashi, J.S. (2014). Molecular architecture of the mammalian circadian clock. Trends Cell Biol *24*, 90–99.

Pickel, L., and Sung, H.K. (2020). Feeding rhythms and the circadian regulation of metabolism. Front. Nutr. *7*, 39.

Rajagopalan, S., Al-Kindi, S.G., and Brook, R.D. (2018). Air pollution and cardiovascular disease: JACC state-of-the-art review. J. Am. Coll. Cardiol. *72*, 2054–2070.

Rajagopalan, S., Park, B., Palanivel, R., Vinayachandran, V., Deiuliis, J.A., Gangwar, R.S., Das, L.M., Yin, J., Choi, Y., Al-Kindi, S., et al. (2020). Metabolic effects of air pollution exposure and reversibility. J. Clin. Invest. *130*, 6034–6040.

Rider, C.F., and Carlsten, C. (2019). Air pollution and DNA methylation: effects of exposure in humans. Clin. Epigenetics *11*, 131.

Russart, K.L.G., and Nelson, R.J. (2018). Light at night as an environmental endocrine disruptor. Physiol. Behav. *190*, 82–89.

Shostak, A., and Brunner, M. (2019). Help from my friends-cooperation of BMAL1 with noncircadian transcription factors. Genes Dev. *33*, 255–257.

Siepka, S.M., Yoo, S.H., Park, J., Song, W., Kumar, V., Hu, Y., Lee, C., and Takahashi, J.S. (2007). Circadian mutant Overtime reveals F-box protein FBXL3 regulation of cryptochrome and period gene expression. Cell *129*, 1011–1023.

Stenvers, D.J., Scheer, F., Schrauwen, P., la Fleur, S.E., and Kalsbeek, A. (2019). Circadian clocks and insulin resistance. Nat. Rev. Endocrinol. *15*, 75–89.

Sun, Q., Yue, P., Deiuliis, J.A., Lumeng, C.N., Kampfrath, T., Mikolaj, M.B., Cai, Y., Ostrowski, M.C., Lu, B., Parthasarathy, S., et al. (2009). Ambient air pollution exaggerates adipose inflammation and insulin resistance in a mouse model of diet-induced obesity. Circulation *119*, 538–546.

Thurman, R.E., Rynes, E., Humbert, R., Vierstra, J., Maurano, M.T., Haugen, E., Sheffield, N.C., Stergachis, A.B., Wang, H., Vernot, B., et al. (2012). The accessible chromatin landscape of the human genome. Nature *489*, 75–82.

Wang, Y., Li, R., Chen, R., Gu, W., Zhang, L., Gu, J., Wang, Z., Liu, Y., Sun, Q., Zhang, K., et al. (2020). Ambient fine particulate matter exposure perturbed circadian rhythm and oscillations of lipid metabolism in adipose tissues. Chemosphere *251*, 126392.

Xia, L., Ma, S., Zhang, Y., Wang, T., Zhou, M., Wang, Z., and Zhang, J. (2015). Daily variation in global and local DNA methylation in mouse livers. PLoS One *10*, e0118101.

iScience, Volume *23*

Supplemental Information

Exposure to Air Pollution Disrupts Circadian Rhythm through Alterations in Chromatin Dynamics

Rengasamy Palanivel, Vinesh Vinayachandran, Shyam Biswal, Jeffrey A. Deiuliis, Roshan Padmanabhan, Bongsoo Park, Roopesh Singh Gangwar, Jared C. Durieux, Elaine Ann Ebreo Cara, Lopa Das, Graham Bevan, Zahi A. Fayad, Ahmed Tawakol, Mukesh K. Jain, Sujata Rao, and Sanjay Rajagopalan

Supplemental Documents

Supplementary Figure 1

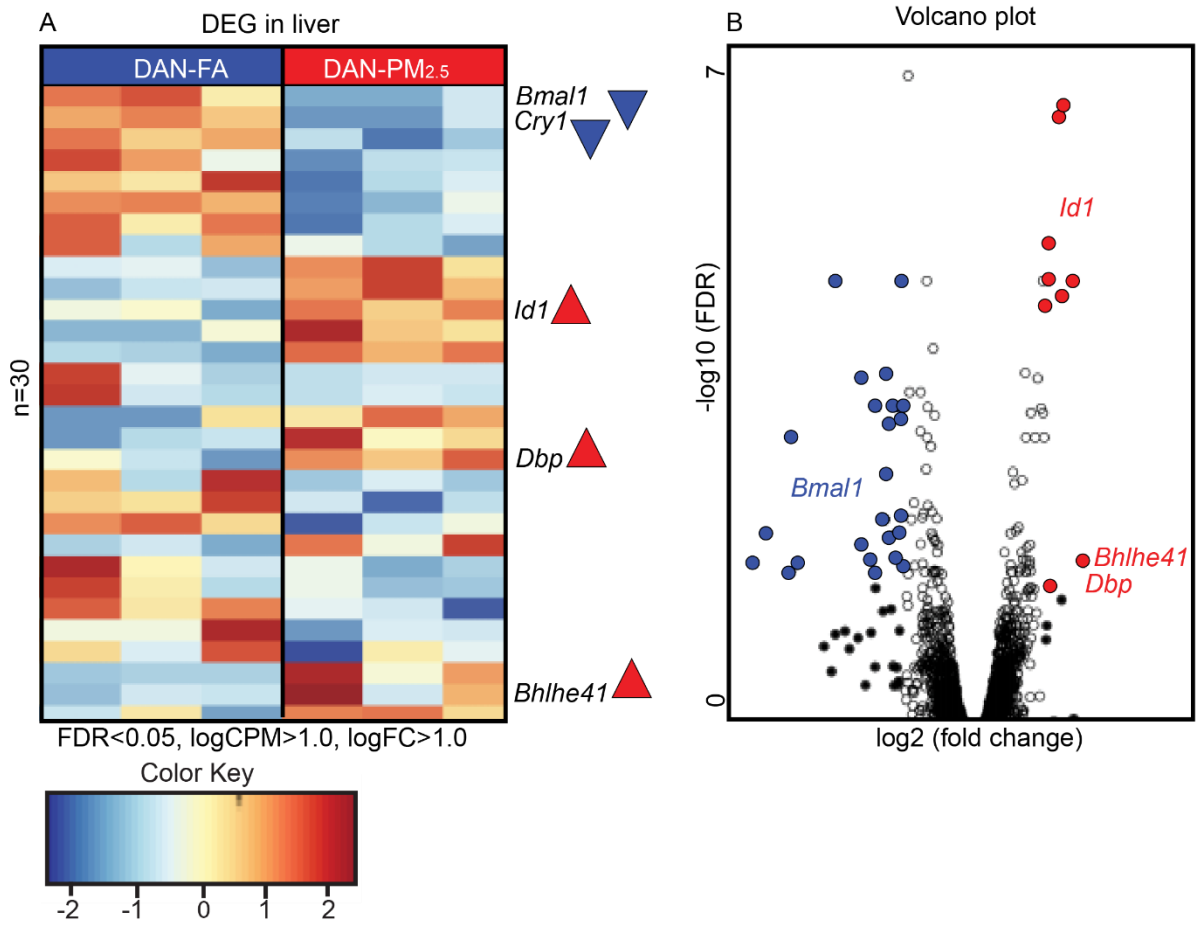

Figure S1. Unbiased transcriptomic analysis of liver samples (ZT02) in mice exposed to $PM_{2.5}$ for 14 weeks, Related to Figure 1

Supplementary Figure 2

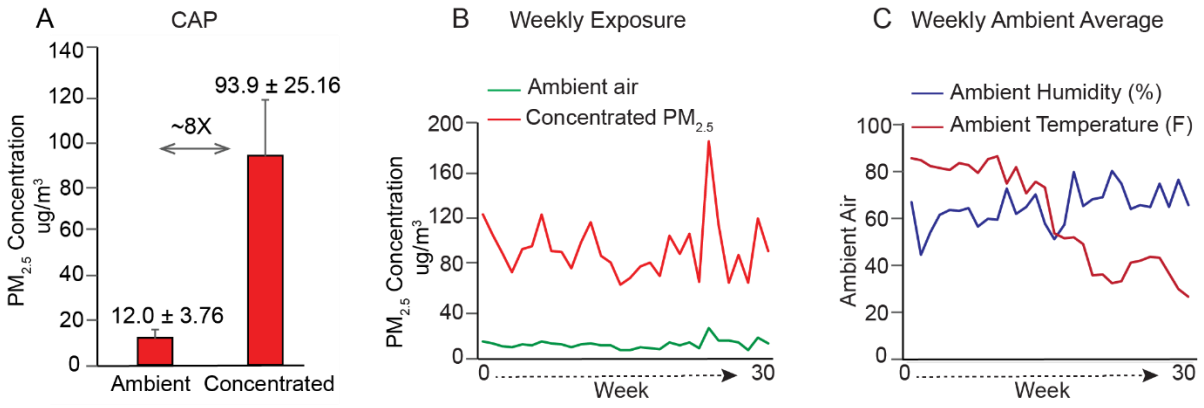

D Level of Elemental Concentration in Ambient vs Concentrated air (Air pollution)

Elements	Ambient Air (ng/cm²) Mean ± SD	Concentrated $PM_{2.5}$ (ng/cm²) Mean ± SD
Na	349.96 ± 39.48	712.98 ± 252.36
Mg	76.31 ± 13.94	187.32 ± 73.29
Al	50.66 ± 37.95	225.38 ± 235.58
Si	37.77 ± 72.68	577.72 ± 506.55
S	75.48 ± 209.77	1870.92 ± 1016.83
Cl	4.37 ± 6.40	10.05 ± 59.99
K	10.75 ± 19.11	176.87 ± 93.36
Ca	34.91 ± 56.82	508.05 ± 412.04
Ti	4.74 ± 3.19	31.94 ± 21.98
Fe	40.84 ± 60.47	736.86 ± 527.86
Cu	5.06 ± 2.06	21.08 ± 15.75
Zn	42.16 ± 20.13	153.71 ± 73.68
Sr	6.34 ± 1.03	8.67 ± 2.73
Zr	3.44 ± 4.22	7.03 ± 6.43
Sn	6.21 ± 7.85	7.57 ± 7.45
Sb	6.04 ± 10.64	10.06 ± 14.01
Te	17.97 ± 20.89	11.23 ± 14.77
Cs	5.06 ± 4.24	0.15 ± 0.80
Lu	7.28 ± 5.31	30.19 ± 13.58
U	67.95 ± 101.93	28.89 ± 53.82
Ni	31.12 ± 2.69	13.10 ± 9.93
Er	3.46 ± 3.14	20.66 ± 11.46
Pb	0.52 ± 1.01	9.99 ± 6.66
W	3.47 ± 3.17	9.24 ± 6.40
P	1.42 ± 2.51	22.67 ± 16.04
Br	1.80 ± 3.30	33.31 ± 72.68

Figure S2. Level of concentrated $PM_{2.5}$ in various groups and elemental composition, Related to Figure 1

Supplementary Figure 3

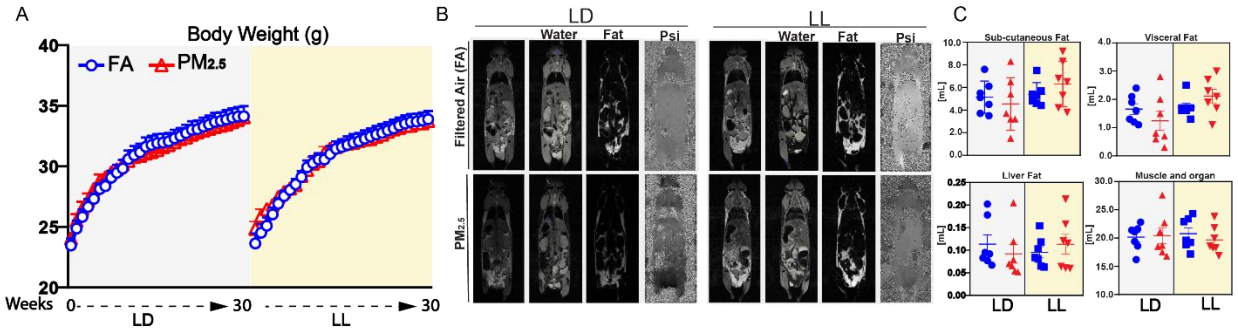

Figure S3. Impact of air-pollution ($PM_{2.5}$) and light at night (LL) on whole body fat mass, Related to Figure 1

Supplementary Figure 4

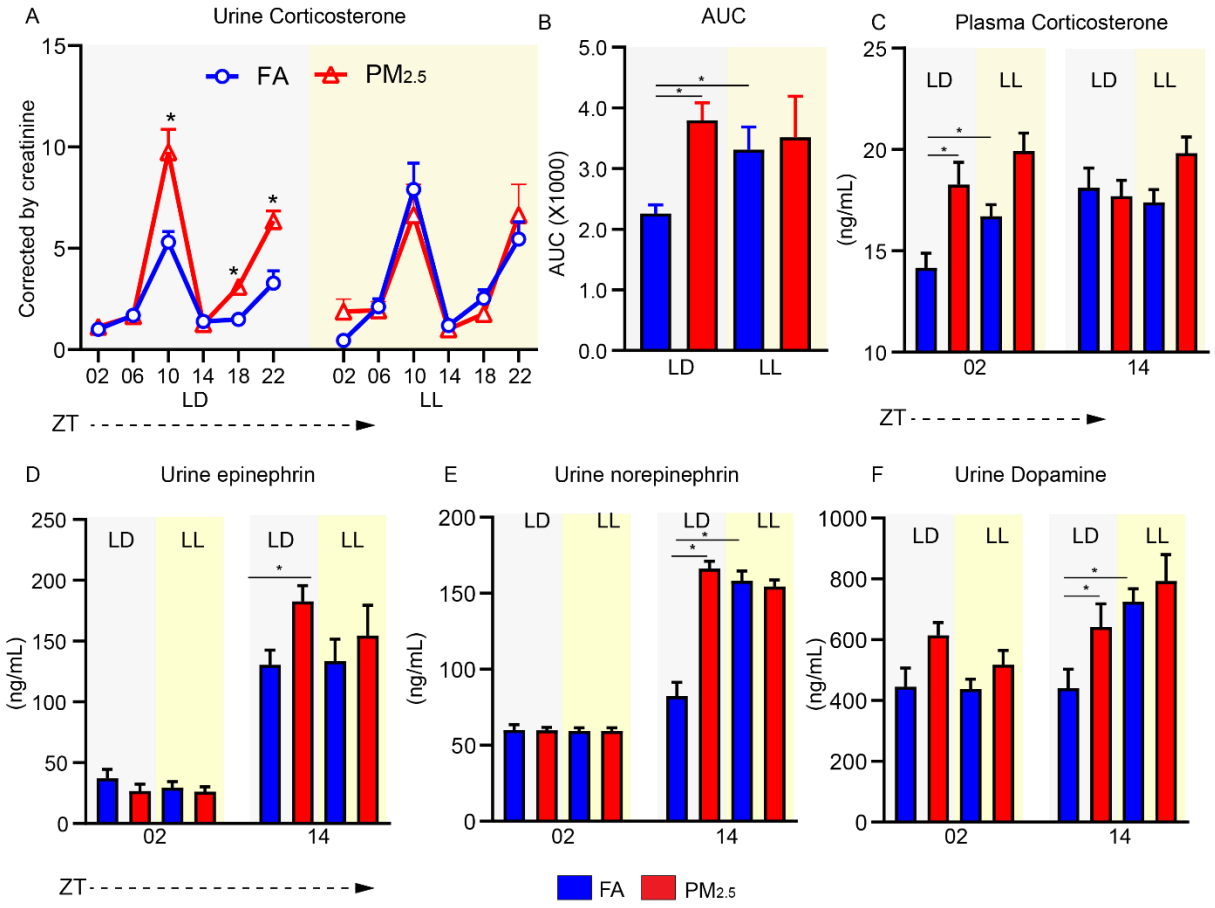

Figure S4. Effect of air-pollution ($PM_{2.5}$) and light at night (LL) on plasma and urinary catecholamine level, Related to Figure 2

Supplementary Figure 5

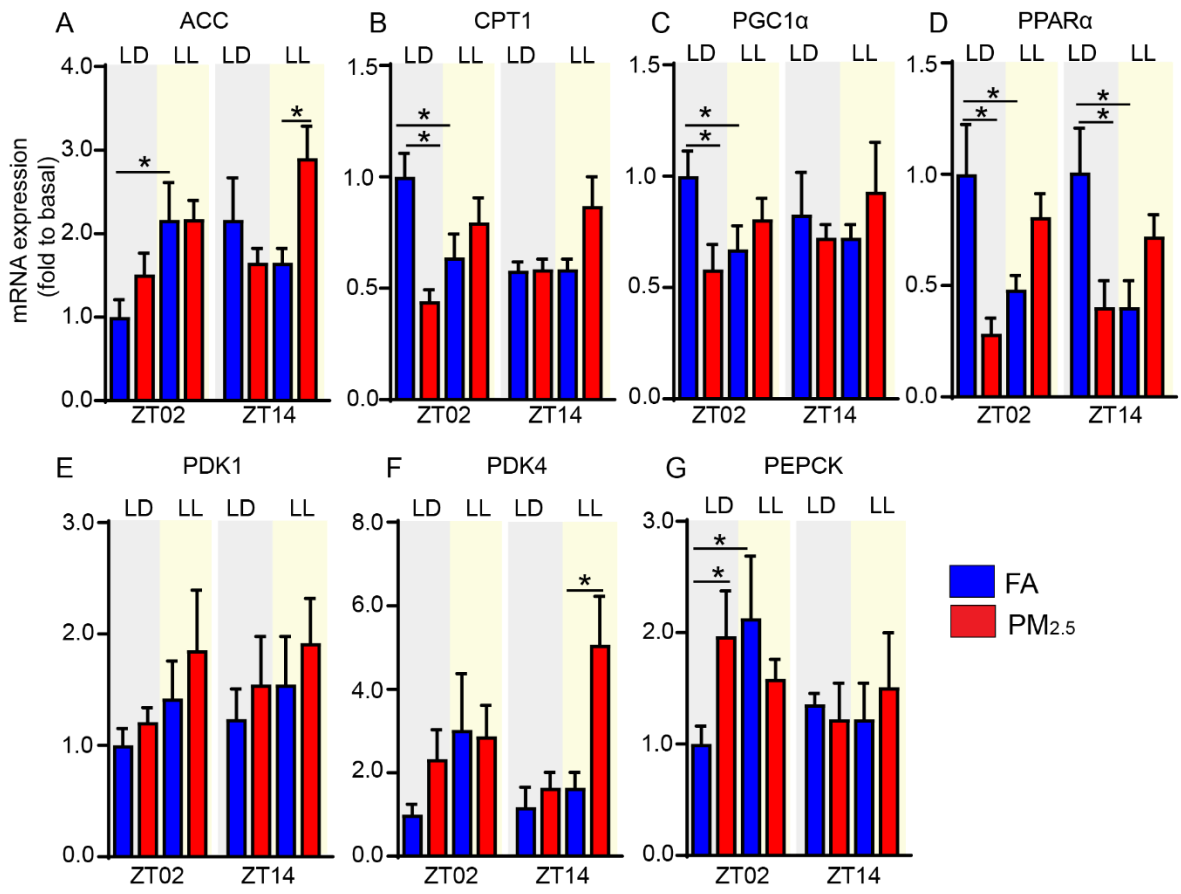

Figure S5. Expression level of metabolically active genes in liver of wild type mice exposed with air-pollution ($PM_{2.5}$) and light at night (LL), Related to Figure 2

Supplementary Figure 6

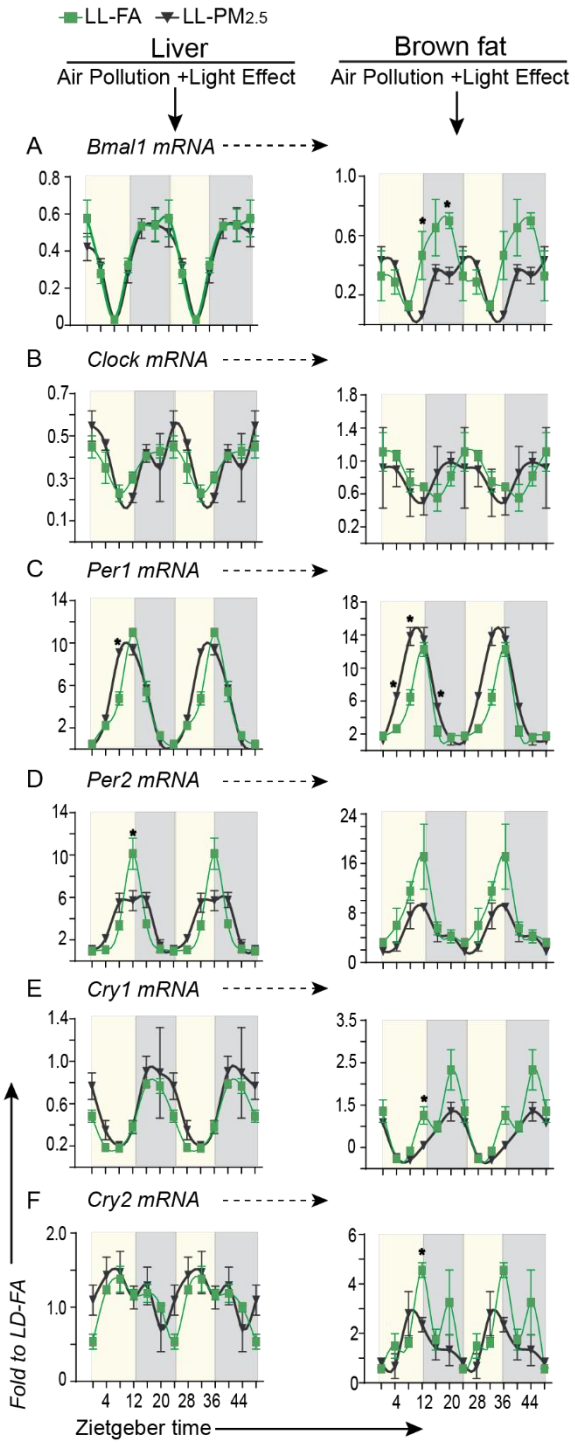

Figure S6. $PM_{2.5}$ plus Light on peripheral circadian rhythm in wild type mice, Related to Figure 2

Supplementary Figure 7

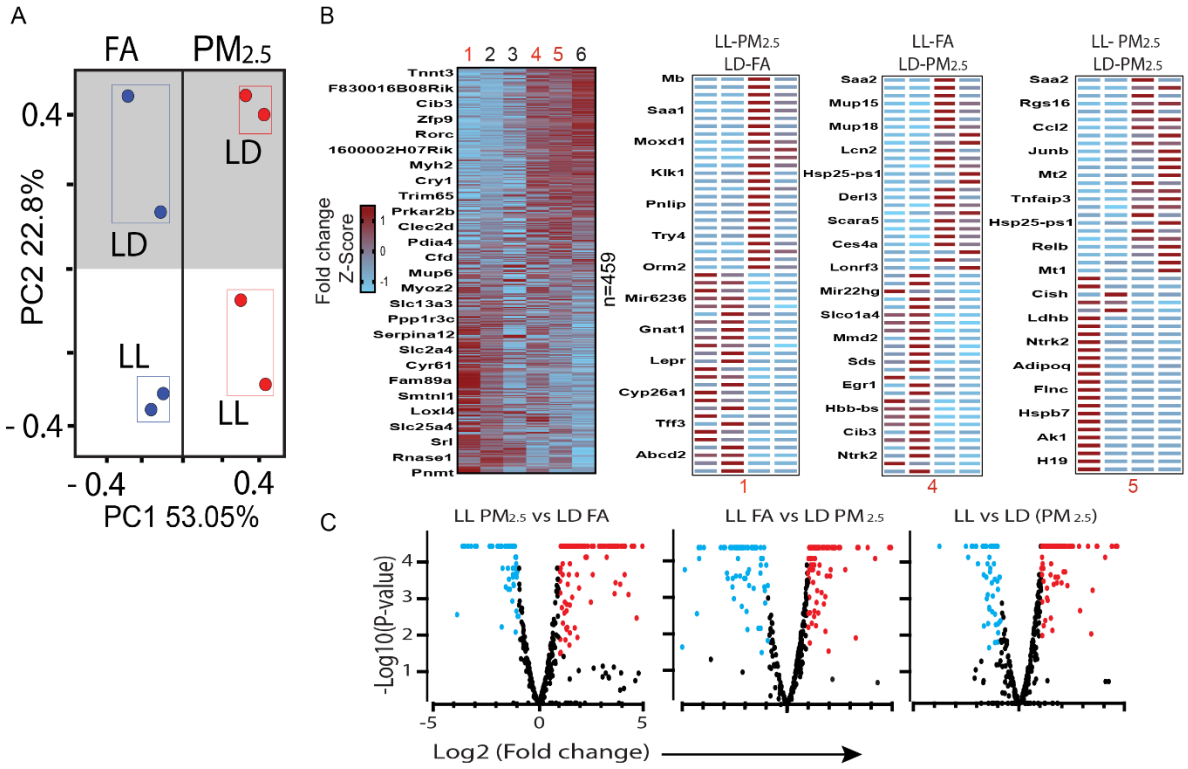

Figure S7. Differential effect of $PM_{2.5}$ and light at night (LL) on liver transcriptome, Related to Figure 3

Supplementary Table 1

Circadian gene		MESOR	p Value	Amplitude	p Value	Acrophase	p Value	Cycling p Value
Bmal1	*LD-FA*	*0.4751475*		*0.4781546*		*23.210186*		*0.00515**
	LD-PM$_{2.5}$	*0.2235200*	*1.20871e-05* [a]	*0.2572473*	*0.00045615* [a]	*20.901409*	*0.000653919* [a]	*0.00905**
	LL-FA	*0.3808750*	*0.009795208* [b]	*0.2664871*	*0.00023165* [b]	*19.996965*	*0.004202895* [b]	*0.04654**
	LL-PM$_{2.5}$	*0.3524100*	*0.279870462*	*0.2345565*	*0.49459407*	*19.997475*	*0.999582386*	*0.04404**
Clock	*LD-FA*	*0.4711575*		*0.3836382*		*22.370084*		*0.04856**
	LD-PM$_{2.5}$	*0.3396225*	*0.036872430* [a]	*0.1591120*	*0.00774965* [a]	*17.386595*	*0.407066262*	*0.17555*
	LL-FA	*0.3607225*	*0.028926914* [b]	*0.1072335*	*0.00124737* [b]	*21.179567*	*0.173478699*	*0.02633**
	LL-PM$_{2.5}$	*0.3644100*	*0.856085727*	*0.1770454*	*0.02970233* [c]	*11.621043*	*0.143700042*	*0.17720*
Per1	*LD-FA*	*4.4871700*		*4.6587179*		*12.093686*		0.21697
	LD-PM$_{2.5}$	*3.0142900*	*0.010469893* [a]	*2.6414670*	*0.00922050* [a]	*12.923761*	*0.230090565*	0.27133
	LL-FA	*4.1883250*	*0.149405844*	*4.6550357*	*0.97823434*	*11.921178*	*0.694543269*	0.05033
	LL-PM$_{2.5}$	*4.649775*	*0.081613087*	*5.1780636*	*0.23105892*	*10.791905*	*0.097955216*	0.00188*
Per2	*LD-FA*	*2.6156725*		*2.4929648*		*12.412633*		0.04938*
	LD-PM$_{2.5}$	*4.0378350*	*0.011507130* [a]	*4.6612373*	*0.03264309* [a]	*12.352367*	*0.927495226*	0.12304
	LL-FA	*3.3550250*	*0.104936630*	*3.8369929*	*0.05141281* [b]	*12.069062*	*0.582640653*	0.11987
	LL-PM$_{2.5}$	*3.5986670*	*0.553462790*	*2.9362332*	*0.19829811*	*11.920924*	*0.821233843*	0.11403
Cry1	*LD-FA*	*0.6518600*		*0.5872745*		*19.723241*		0.00709*
	LD-PM$_{2.5}$	*0.4611925*	*0.025545406* [a]	*0.1964905*	*0.00298631* [a]	*20.152340*	*0.702949206*	0.19075
	LL-FA	*0.4634350*	*0.024643128* [b]	*0.3491752*	*0.02801319* [b]	*18.386989*	*0.099875546*	0.00192*
	LL-PM$_{2.5}$	*0.5822700*	*0.124363775*	*0.4158133*	*0.70669751*	*15.154233*	*0.521417173*	0.01544*
Cry2	*LD-FA*	*1.3202800*		*0.4781722*		*13.018262*		0.03312*
	LD-PM$_{2.5}$	*1.2162175*	*0.621442695*	*0.4071473*	*0.59094435*	*8.3898884*	*0.046945202* [a]	0.39293
	LL-FA	*1.0841250*	*0.131232826*	*0.3007884*	*0.16074719*	*10.272730*	*0.023742458* [b]	0.25913
	LL-PM$_{2.5}$	*1.1878725*	*0.514822831*	*0.3606528*	*0.20918143*	*8.1397044*	*0.244456881*	0.23006

Table S1. Cosinor analysis of circadian genes in liver, Related to Figure 2

Supplementary Table 2

Circadian gene		MESOR	p Value	Amplitude	p Value	Acrophase	p Value	Cycling p Value
Bmal1	*LD-FA*	*0.5821500*		*0.6853124*		*21.530963*		0.00851*
	LD-PM$_{2.5}$	*0.3038200*	*0.002594268* [a]	*0.3031707*	*0.00510237* [a]	*22.558070*	*0.242813991*	0.03124*
	LL-FA	*0.4272600*	*0.093637845*	*0.3365980*	*0.01085447* [b]	*18.305526*	*0.094588572*	0.03367*
	LL-PM$_{2.5}$	*0.2787175*	*0.037792743* [c]	*0.1830650*	*0.03929240* [c]	*22.717388*	*0.026670530* [c]	0.12201
Clock	*LD-FA*	*0.9086000*		*0.3871367*		*21.297822*		0.04230*
	LD-PM$_{2.5}$	*0.7749100*	*0.079960450*	*0.4503129*	*0.67776922*	*16.818658*	*0.114922991*	0.07101
	LL-FA	*0.8288100*	*0.307560990*	*0.3313560*	*0.73352477*	*7.6363178*	*0.046405087* [b]	0.08610
	LL-PM$_{2.5}$	*0.7934325*	*0.828200913*	*0.4418717*	*0.34566122*	*13.517189*	*0.438437759*	0.05307
Per1	*LD-FA*	*3.2319550*		*2.8540918*		*10.970798*		0.18724
	LD-PM$_{2.5}$	*5.4244900*	*0.009184235* [a]	*6.6456521*	*0.01193468* [a]	*10.657929*	*0.473685066*	0.09304
	LL-FA	*4.4973250*	*0.026183497* [b]	*4.5341405*	*0.10478281*	*10.765168*	*0.623734731*	0.16854
	LL-PM$_{2.5}$	*6.9292800*	*0.031107098* [c]	*7.1509239*	*0.08483440*	*9.7282170*	*0.117572427*	0.00335*
Per2	*LD-FA*	*5.5682800*		*6.0155055*		*15.055741*		0.04731*
	LD-PM$_{2.5}$	*3.8727700*	*0.229019036*	*3.7949755*	*0.31544190*	*14.184400*	*0.393365511*	0.19858
	LL-FA	*7.9235450*	*0.197950379*	*6.2111323*	*0.91310225*	*10.555955*	*1.40345e-05* [b]	0.08589
	LL-PM$_{2.5}$	*4.9585725*	*0.043436820* [c]	*3.9118945*	*0.06504908*	*11.635098*	*0.417037191*	0.06571
Cry1	*LD-FA*	*1.1916275*		*1.4510653*		*19.372820*		0.03471*
	LD-PM$_{2.5}$	*0.6640700*	*0.002828390* [a]	*0.6520268*	*0.010979775* [a]	*18.309051*	*0.532259820*	0.04413*
	LL-FA	*1.0986325*	*0.508046290*	*0.8333420*	*0.029669969* [b]	*18.918508*	*0.529200260*	0.17684
	LL-PM$_{2.5}$	*0.7328075*	*0.024801920* [c]	*0.5907753*	*0.128065244*	*19.765730*	*0.236281690*	0.03133*
Cry2	*LD-FA*	*2.6129025*		*2.7754165*		*17.409901*		0.08550
	LD-PM$_{2.5}$	*1.4265425*	*0.016264978* [a]	*1.0171037*	*0.005313846* [a]	*16.856182*	*0.7858926630*	0.35483
	LL-FA	*2.2101400*	*0.320025389*	*1.4079303*	*0.030145224* [b]	*14.365625*	*0.0770324520*	0.42185
	LL-PM$_{2.5}$	*1.5626150*	*0.122093005*	*1.1280335*	*0.522138861*	*12.255406*	*0.3315054400*	0.16734

Table S2. Cosinor analysis of circadian genes in BAT, Related to Figure 2

Supplementary Table 3

Primer	Forward	Reverse
Clock	5'-GAGGTCGTCCTTCAGCAGTC -3'	5'-TGTGACATGCCTTGTGGAAT -3'
Bmal1	5'-AAGTGCAACAGGCCTTCAGT - 3'	5'-GGTGGCCAGCTTTTCAAATA -3'
Per1	5'-CCAGGATGTGGGTGTCTTCT -3'	5'-TTTCCTGGGTGAAGTCCTTG -3'
Per2	5'-ATTGGGAGGCACAAAGTCAG -3'	5'-CAGTAGCCGGTGGATTTGTT -3'
Cry1	5'-TTCACTGCTACTGCCCTGTG -3'	5'-TTTTGCAGGGAAGCCTCTTA -3'
Cry2	5'-ATGTGTTCCCAAGGCTGTTC -3'	5'-CCTCCTTGGCCATCTTCATA -3'
ACC	5'-GGATGACAGGCTTGCAGCTAT -3'	5'-TTTGTGCAACTAGGAACGTAAGTCG -3'
PDK1	5'-TCCTGTCACCAGCCAAAATG -3'	5'-CCACCGAACAATAAGGAGTGC -3'
PDK4	5'-GAGGATTACTGACCGCCTCTTTAG -3'	5'-TTCCGGGAATTGTCCATCAC -3'
PEPCK	5'-CCCTTGTCTATGAAGCCCTCA -3'	5'-GCCGAAGTTGTAGCCGAAGA -3'
PPARα	5'-ACACTGCCAAGGAGTCGAG -3'	5'-AGGCATCTACCACCATGTCCATAA -3'
PPARγ	5'-AGCTGACCCAATGGTTGCTGATTA -3'	5'-GGAGATGCAGGTTCTACTTTGATCG -3'
CPT1	5'-CTGCTGCATGGTAGATGTTTCGAC -3'	5'-GCCCAGGAATGCTCTGCGTTTA -3'
PGC1α	5'-AGCCGTGACCACTGACAACGAG -3'	5'-GCTGCATGGTTCTGAGTGCTAAG -3'
UCP1	5'-GGCATTCAGAGGCAAATCAGCT -3'	5'-CAATGAACACTGCCACACCTC -3'
PRDM16	5'-CCACCAGCGAGGACTTCAC -3'	5'-GGAGGACTCTCGTAGCTCGAA -3'
HDAC1	5'-AGTCTGTTACTACTACGACGGG' -3	5'-TGAGCAGCAAATTGTGAGTCAT -3'
HDAC2	5'-GCGTACAGTCAAGGAGGCGGC' -3	5'-GGCTTCATGGGATGACCCTGGC' -3'
HDAC3	5'-CACCAAGAGCCTTGATGCCTT' -3	5'-GCAGCTCCAGGATACCAATTACT' -3'
HDAC4	5'-TGAGAGACGGAGCAGCCCCC -3	5'-TGGAGAGCTGGGACCGGAGC -3'
DNMT1	5'-CCTAGTTCCGTGGCTACGAGGAGAA -3	5'-TCTCTCTCCTCTGCAGCCGACTCA -3'
DNMT3A	5'- GCCGAATTGTGTCTTGGTGGATGACA' -3	5'-CCTGGTGGAATGCACTGCAGAAGGA -3'
GAPDH	5'- AACGACCCCTTCATTGAC' -3	5'-TCCACGACATACTCAGCAC -3'
RPL13A	5'-GGAGAAACGGAAGGAAAAGG -3'	5'-GAGTCCGTTGGTCTTGAGGA -3'
B2M	5'-TGGTGCTTGTCTCACTGACC -3'	5'-TATGTTCGGCTTCCCATTCT -3'

Table S3. Mouse primers used for Circadian Rhythm and Metabolic Study, Related to Figure 2, Figure 5 and Fig S5 and Fig S6

Transparent Methods

Exposure of Animals to Ambient $PM_{2.5}$

Laboratory mice were exposed to concentrated ambient $PM_{2.5}$ or filtered air (FA) using a Versatile Aerosol Concentration Enrichment System (VACES) whose laboratory and field characterization have been previously described in detail (Chen, 2003) (Maciejczyk and Chen, 2005; Sun et al., 2009). VACES allows the concentration of ambient particulates in the atmosphere in Cleveland, Ohio, USA, allowing chronic inhalational exposure of mice in chambers to concentrated ambient particulate matter <2.5 microns (CAP) in diameter. Briefly, the sampled ambient aerosol from VACES located in metropolitan Cleveland is drawn inside a saturator and mixed with ultrapure deionized water vapor to achieve saturation, following which it passes through a cooling section that induces condensational growth of the particles to super-micrometer size via supersaturation. The grown particles are then concentrated by virtual impaction. VACES employs three virtual impactors in parallel, achieving an overall enrichment factor of 10-20x, depending on ambient concentration levels. The particles themselves are analyzed after collection on Teflon filters using XRF (X-ray fluorescence, a non-destructive analytical technique) analysis to determine the elemental composition of deposited $PM_{2.5}$. The elemental composition during exposure for this experiment is depicted in Supplemental Figure 2. For the initial discovery study, three-week-old C57BL/6J male mice were purchased from the Jackson Laboratories (Bar Harbor, ME), and were equilibrated for 1 week prior to experimental enrollment. Weight matched mice were then divided into two groups and exposed to either filtered air (FA) and/or concentrated $PM_{2.5}$ at nominal 10 × (80-100μg/m^3) ambient concentrations 6 hours per day, 5 days per week in standard light-dark cycle (12 h day light/12 h dark) (LD) with concomitant *ad libitum* access to standard chow diet for 14 weeks. For the validation study, three-week-old C57BL/6J male mice were equilibrated for 1

week prior to experimental enrollment and divided into four groups; (1) LD-FA (12h day light/12h dark and received filtered air daily 6h/day/5 days in a week). (2) LD-$PM_{2.5}$ (12h day light/12h dark and received concentrated $PM_{2.5}$ air daily 6h/day/5 days in a week). (3) LL-FA (12h day light/12h dim light and received filtered air daily 6h/day/5 days in a week) and (4) LL-$PM_{2.5}$ (12h day light/12h dim light and received concentrated $PM_{2.5}$ air daily 6h/day/5 days in a week) with concomitant *ad libitum* access to standard chow diet for 30 weeks. The control (FA) mice in the experiment were exposed to an identical protocol with the exception of a high-efficiency particulate-air (HEPA) filter positioned in the inlet valve position to remove all of the $PM_{2.5}$ in the filtered air stream. All the animal experiments were approved by the Case Western Reserve University IACUC committee and carried out under the institutional guidelines for ethical animal use.

Glucose and Insulin Tolerance Test

Basal blood glucose was measured after 12h of fasting using a handheld glucometer (Contour). Mice were given an intraperitoneal bolus of glucose (glucose tolerance test) or insulin (insulin tolerance test) at a concentration of 2 mg/kg or 0.75 IU/kg body weight, respectively, and blood glucose was measured at 20, 40, 60, 90 and 120 minutes thereafter.

Blood Glucose, Plasma Insulin

Retro-orbital blood was collected under isoflurane anesthesia after 12 hours of fasting. Whole-blood glucose was determined by using the glucometer (Contour) with glucose test strips as described by the manufacturer. Plasma insulin was determined by using a mouse insulin ELISA kit with mouse insulin as a standard (Alpco, Salem, NH03079). The homeostatic model assessment of insulin resistance (HOMA-IR) was calculated using the equation [(Glucose × Insulin)/405].

Urine and Plasma Corticosteroid Assay

Catecholamine levels such as epinephrine, nor-epinephrine and dopamine (3-CAT ELISA assay kit, Rocky Mountain Diagnostic Inc., Colorado Springs, CO 80903, USA) and total corticosterone level (Life Technology Corporation, Frederick, MD, USA) were measured according to the manufacturer instructions. Briefly, urine from different groups of mice were collected at ZT2, ZT6, ZT10, ZT14, ZT18, and ZT22 time points and stored at -80^{o}C or used for catecholamine and total corticosterone measurement. For plasma total corticosterone levels, blood collected at ZT2 and ZT14 was used for this assay.

***In vivo* Glucose Uptake Measured by Positron Emission Tomography**

[18F] Fluorodeoxyglucose (FDG) was purchased from PETNET solution (Cleveland, USA) and a cyclotron (Siemans20–30 gb). After an 8 h fast mice were injected with insulin (0.75 U/kg) diluted in 0.9% physiological saline and 5 min later received an intravenous administration of FDG (200-300μCi). After injection, the mice were maintained under conscious conditions and warmed using a heating pad. Before PET imaging, a CT scout view was taken to ensure mice were placed in the co-scan field of view (FOV) where the highest image resolution and sensitivity are achieved. Once the static acquisition was done, a CT acquisition scan was performed for attenuation correction. At 30 min small-animal positron emission tomography (uPET/CT, Siemens Medical solution Inc, TN 37932, USA) and micro-computed tomography (CT) (uPET/CT: Inveon, Siemens Medical solution Inc, TN 37932, USA) imaging were performed using an acquisition time of 15-30 min for PET at Case Center for Imaging Research (CCIR). Quantitative image analysis of the uptake of ^{18}F-FDG in different organs was performed using Carimas II software. This program allows the regions of interest (ROI) to be extrapolated from the reconstructed uPET image frames, allowing the quantification of the SUV (standard uptake value) in a specific region. Based on the PET and

CT co-registered images, brain, liver, heart, muscle, WAT and BAT were then defined as (ROI) and FDG tissue uptake calculated using the mean value of standard uptake values (SUV).

Body Composition and Indirect Calorimetry

In vivo body composition analysis of lean mass and fat mass from conscious, immobilized mice was performed by the Case Center for Imaging Research (CCIR). The data and images were collected as described previously (Johnson et al., 2012) by using Bruker Biospec 7T small animal MRI scanner (Bruker Biospin, Billerica, MA). For indirect *in vivo* metabolic analyses, 20 weeks of FA/$PM_{2.5}$-exposured mice were acclimated to the apparatus for 24 hours before data collection commenced, after which energy expenditure was measured using a computer-controlled indirect calorimetry system (Oxymax Comprehensive Lab Animal Monitoring System, Columbus Instruments, Columbus, OH), run by the MMPC (Mouse Metabolic Phenotyping Core) at Case Western Reserve University (CWRU). For each animal, O_2 consumption and CO_2 production were measured for 1 min at 10-min intervals. Respiratory Quotient (RQ) was calculated as the ratio of CO_2 production to O_2 consumption. Energy expenditure was calculated using the Weir equation with normalization to body weight. Light and dark cycle energy expenditure was determined using the average of all data points per 12-h light/dark cycle of 2 consecutive days, and these, in turn, were averaged to obtain total 24-h energy expenditure. Data acquisition and instrument control were coordinated by MetaScreen and raw data was processed using ExpeData with an analysis script documenting all aspects of data transformation.

Quantitative Real-Time RT-PCR (qPCR) Analysis

Total RNA was extracted from liver and brown fat using Trizol® Reagent (Life Technologies, Grand Island, NY). cDNA was synthesized using Transcriptor First Strand cDNA synthesis kit (Roche Applied Science, Indianapolis, IN) according to the manufacturer's protocol. The

amplification of target genes was used by a LightCycler® 480 SYBR Green I Master kit (Roche Applied Science, Indianapolis, IN). Gene expression was measured by quantitative real-time PCR performed on a LightCycler® 480 real-time PCR System (Roche Applied Science, Indianapolis, IN). The sequences of real-time PCR primers used in this study are shown in Supplementary Table 3. Fold changes of mRNA levels were determined using the ΔΔCt method and normalized to internal control GAPDH, RPL13 and B2M.

RNA-Sequencing

The extracted RNA was quantified by NanoDrop (Thermo Fisher Scientific, MA) and the quality was assessed using a 2100 Bioanalyzer (Agilent Technologies, CA). The Agilent Bioanalyzer is a microfluidics platform used for sizing, quantification, and quality control for RNA (and DNA/ proteins) and provides an "RNA Integrity Number" (RIN), which quantifies the fragmentation of the RNA sample. The RNA samples were selected for sequencing if RIN value was more than 6.5. On average, 500-1,000 mg of RNA samples were used for library preparation and double-stranded cDNA generation. We utilized the NEBNext® Ultra RNA Library Prep Kit (New England BioLabs, Inc, Ipswich, MA) for liver tissues and a TrueSeq RNA Library Prep Kit (Illumina, San Diego, CA) to generate strand-specific libraries for all other mentioned issues. The library was amplified by 15-cycle according to the manufacturer protocol. After PCR primers removal with Agencourt AMPure PCR purification kit (Beckman Coulter, CA), the sequencing library was quantified on TapeStation (TapeStation Instrument). The prepared library was sequenced by HiSeq series sequencer including HiSeq4000, HiSeqX (Illumina, San Diego, CA). The raw BCL files were converted into FastQ files using CASAVA 1.8.2 (CASAVA).

Transcriptome Analysis

A total of 500 million reads were used, with an average of 50 million reads per sample. We built an index sequence for STAR using the Gencode M13 reference feature that includes protein-coding genes as well as non-coding genes. In total, 50,600 genes and 124,031 transcripts including isoforms were identified. Prior to sequence alignment, we applied trimgalore (version 0.4.3) with cut adapt package (version 1.12) (Martin, 2011) for removing any unnecessary genomic fragments (e.g. adapter dimers) and low quality nucleotide sequences from the raw reads. We mapped raw sequencing reads to the mouse reference genome (mm10) using STAR aligner 7, and calculated the raw count using feature Counts package (Risso et al., 2014). Finally, we extracted gene level transcripts (N=50,600) and transcript level isoforms (N=124,031) using the feature Counts. To test reproducibility and examine outlier samples, we conducted PCA analysis and MDR block analysis, as well as pair-wise comparative analysis showing the correlation scores in a matrix format (Fig. S1). We excluded extreme outlier samples before conducting differentially expressed gene analysis. All datasets are deposited under GEO accession number (GSE145566) and are accessible to the scientific community.

Differentially Expressed Genes (DEGs)

We used protein coding genes and long non-coding RNA from Gencode M13 (Freeze date Oct 2016). For transcriptome analysis, we were primarily interested in assaying gene-level expression (protein-coding genes). We used Rsub read and feature counts to generate a gene-by-sample matrix of reading counts that was analyzed using edgeR after removing unwanted variation (RUVg) (Risso et al., 2014). The output of this analysis is a set of genomic regions that are significantly different between the experimental groups. For transcript level expression analysis, we also utilized the alignment free mapping method in Salmon to quantify the number of transcripts and

transcript per million (TPM). We compared gene-level DEGs and transcript level DEGs and summarized the results in Supplementary Table 4. Due to the small number of biological replicates (N=2), we utilized the limma based edgeR method to determine differentially expressed transcripts or isoforms; cutoff: log2FC > 0.7 for liver and adipose samples (log CPM>0.7, FDR < 0.05). We used a low threshold in fold change (low-fold change DEGs: log2FC between 0.7 and 1.0) due to the potentially small effect size of environmental exposure on epigenome or transcription, resulting in only small variations in the transcriptome. We performed GO and Pathway analysis using DEGs and control genes. We used R Package Top GO 9 to generate the GO and GSEA to generate KEGG/Reactome pathways. In addition, we performed IPA (Ingenuity Systems Inc., Redwood City, CA) to check for enriched pathways from DEGs and search for upstream regulators (TF, enzyme, receptors). To validate our findings Transfac, and HOMER analysis 10 were performed to confirm upstream regulators from the DEGs list.

Open Chromatin Signatures from Liver Samples using ATAC-seq

Livers from 14-week-exposed male mice were harvested and the left lobe of liver was pulverized. Using same Freezer Mill (6775 Freezer/Mill® Cryogenic Grinder) that was used in RNA-seq library prep, 20-30 mg of frozen liver powder was used for prepare ATAC-seq library. The OMNI ATAC-seq protocol (Corces et al., 2017) was adopted for isolating nuclei and applying transposase reaction. The library was purified using two-sided SPRI beads selection (100-500bp fragment size). We utilized Hi-Seq system to sequence the libraries. Due to the limitation of the original protocol, we have relatively high background noise (compare to the advanced OMNI ATAC-seq protocol) (Martin, 2011) and less number of reads under the predicted peaks (open chromatin). Briefly, all reads were trimmed using cut adapt package, and trimmed read (>36bp minimum alignment length) have been mapped against mm10 genome using BWA aligner (Li and Durbin,

2009). The candidate peaks were predicted by MACS peak calling software (Zhang et al., 2008). Parameters used for open chromatin peaks (-g mm -q 0.01 –keep-dup 1000 –no model –shift 0 -extsize 150), fine grain and smaller peaks (-extsize 40). We used predicted open chromatin peaks where at least two biological replicates were reproducible for the downstream analysis using IDR cutoff 0.05.(Q Li, 2011) All the pipeline is freely available via git hub and docker image developed by Bo Zhang lab at WASHU (https://hub.docker.com/r/zhanglab/atac-seq/). Finally, the open chromatin regions were submitted to search potential transcription factor binding sites using HOMER (Heinz et al., 2010) software (mm10 -size 150 -len 11). We collected high-confidence candidate motifs (p-value < 1e-10) using Homer known motif search.

ChIP-qPCR Assay

Mice liver were collected as described in the previous section, livers from two mice from each group (LD-FA, LD-$PM_{2.5}$, LL-FA, LL-$PM_{2.5}$) were used to prepare chromatin. Briefly, liver tissues (10-15mg) were fixed with 1% formaldehyde at room temperature for 15 min with swirling and quenched with 0.125M glycine for 5 min at room temperature. Cross-linked tissues were lysed in high salt buffer for 15 min in ice and subsequently nuclear lysis with SDS for 10 min in ice. Nuclear lysed extracts were subjected to sonication 30s on and 30s off using Diagenode Pico for 20-30 cycles at 4^{o}C. After sonication DNA fragment size was checked in aliquots of sonicated extract, after protease treatment and reverse crosslinking at 65^{0} C overnight. For each ChIP, 3-5ug of ChIP grade antibodies such as Bmal1 Ab3350, Clock Ab3517, p300 sc48343, pCAFsc8999 and Pol-II Millipore 05-623B were used, blocked with BSA and cross-linked on magnetic protein A/G based on the antibody of origin, at 4^{o}C for 4hr. After sonication, the lysate was checked with desirable DNA fragment size (200-800bp) and incubated with the antibody at 4^{o}C overnight. The ChIP complex was pulled down using a magnetic separator and washed with high sucrose buffer, high

salt buffer, LiCl buffer with protease inhibitor and with a final Tris wash. The immune complex was eluted and reverse cross-linked at 65^0 overnight, phenolysed and ethanol precipitated. DNA amount was quantified using qubit and the immune precipitate is quantified with no antibody as control using qPCR and desired primer for Per1 and Per2 (Supplementary Table3).

Statistics

Unless otherwise noted, values presented are expressed as means ± SEM. Statistical analyses were performed using student t-test, one- and two-way analysis of variance (ANOVA) using SAS 9.4 statistical programming. Significance was set at $P < 0.05$. The Cosinor method was used to investigate the presence of a daily 24 h rhythm. The method consists of adjusting a cosine curve to the actual 24 h time series (Cosinor method). The null hypothesis tested was that of zero amplitude, that is, no rhythmicity at the assumed frequency (24 h). A significant periodic fit was considered when the *P* value was <0.05.

References

Chen, L.C., Zhong, M. Narciso, S.P., M. Kleinman, M., C. Nadziejko, C., and Lippmann, M. (2003). Methods for Exposing Rodents and Cells to Concentrated Ambient PM using a VACES. In American Association for Aerosol Research - Particulate Matter Conference (Pittsburgh, PA.).

Corces, M.R., Trevino, A.E., Hamilton, E.G., Greenside, P.G., Sinnott-Armstrong, N.A., Vesuna, S., Satpathy, A.T., Rubin, A.J., Montine, K.S., Wu, B., et al. (2017). An improved ATAC-seq protocol reduces background and enables interrogation of frozen tissues. Nat. Methods *14*, 959-962.

Heinz, S., Benner, C., Spann, N., Bertolino, E., Lin, Y.C., Laslo, P., Cheng, J.X., Murre, C., Singh, H., and Glass, C.K. (2010). Simple combinations of lineage-determining transcription factors

prime cis-regulatory elements required for macrophage and B cell identities. Molecular cell *38*, 576-589.

Johnson, D.H., Narayan, S., Wilson, D.L., and Flask, C.A. (2012). Body composition analysis of obesity and hepatic steatosis in mice by relaxation compensated fat fraction (RCFF) MRI. J. Magn Reson. Imaging *35*, 837-843.

Li, H., and Durbin, R. (2009). Fast and accurate short read alignment with Burrows-Wheeler transform. Bioinformatics *25*, 1754-1760.

Maciejczyk, P., and Chen, L.C. (2005). Effects of subchronic exposures to concentrated ambient particles (CAPs) in mice. VIII. Source-related daily variations in in vitro responses to CAPs. Inhal. Toxicol *17*, 243-253.

Martin, M. (2011). Cutadapt Removes Adapter Sequences From High-Throughput Sequencing Reads. EMBnet.journal *17*.

Q Li, J.B., H Huang, PJ Bickel (2011). Measuring reproducibility of high-throughput experiments. Ann. Appl. Stat *5*, 1752-1779.

Risso, D., Ngai, J., Speed, T.P., and Dudoit, S. (2014). Normalization of RNA-seq data using factor analysis of control genes or samples. Nat. Biotechnol *32*, 896-902.

Sun, Q., Yue, P., Deiuliis, J.A., Lumeng, C.N., Kampfrath, T., Mikolaj, M.B., Cai, Y., Ostrowski, M.C., Lu, B., Parthasarathy, S., et al. (2009). Ambient air pollution exaggerates adipose inflammation and insulin resistance in a mouse model of diet-induced obesity. Circulation *119*, 538-546.

Zhang, Y., Liu, T., Meyer, C.A., Eeckhoute, J., Johnson, D.S., Bernstein, B.E., Nusbaum, C., Myers, R.M., Brown, M., Li, W., et al. (2008). Model-based analysis of ChIP-Seq (MACS). Genome Biol *9*, R137.